SINGULAR VECTORS, METRICS AND ADAPTIVE OBSERVATIONS

by

T.N. Palmer, R. Gelaro*, J. Barkmeijer and R. Buizza

ECMWF, Reading, UK
* Naval Research Laboratory, Monterey, California 93943, USA

Abstract

Singular vectors of the linearised equations of motion have been used to study the instability properties of the atmosphere-ocean system, and also its related predictability. A third use of these singular vectors is proposed here: as part of a strategy to target adaptive observations to "sensitive" parts of the atmosphere. Such observations could be made using unmanned aircraft, though calculations in the paper are motivated by the upstream component of the Fronts and Atlantic Storm-Track Experiment (FASTEX). Oceanic applications are also discussed. In defining this strategy, it is shown that there is, in principle, no freedom in the choice of inner product or metric for the singular vector calculation. However, the correct metric is dependent on the purpose for making the targeted observations (to study precursor developments or to improve forecast initial conditions). It is argued that for predictability studies, where both the dynamical instability properties of the system and the specification of the operational observing network and associated data assimilation system are important, the appropriate metric will differ from that appropriate to a pure geophysical fluid dynamic (GFD) problem. Based on two different sets of calculations, it is argued that for predictability studies (but not for GFD studies), a first order approximation to the appropriate metric can be based on perturbation energy. The role of observations in data assimilation procedures (constraining large scales more than small scales), is fundamental in understanding reasons for the requirement for different metrics for the two classes of problem. An index-based tensor approach is used to make explicit the role of the metric in adjoint-based calculations.

The strategy for using singular vectors to target adaptive observations is discussed in the context of other possible approaches; specifically, based on breeding vectors, potential vorticity diagnosis, and sensitivity vectors. The basic premises underlying the use of breeding and singular vectors are discussed. A comparison of the growth rates of breeding and singular vectors is made using a T21 quasi-geostrophic model.

Singular vectors and subjective potential vorticity diagnosis are compared for a particular case study. The areas of sensitivity indicated by the two methods only partially agree. Reasons for disagreement hinge around the fact that subjective PV diagnosis emphasise lagrangian advection, whilst singular vector analysis emphasises wave propagation. For the latter, areas of sensitivity may be associated with regions of weak PV gradient e.g. in the mid-lower troposphere. Amplification of singular vectors propagating from regions of weak PV gradient to regions of strong PV gradient is discussed in terms of pseudo momentum conservation. Evidence is shown that analysis error may be as large in the lower-mid troposphere as in the upper troposphere.

1. INTRODUCTION

In this paper we consider the dominant singular vectors (or optimal vectors) of the integral tangent propagator, $\boldsymbol{L}$, for a nonlinear dynamical system A, such as the atmosphere, or the coupled ocean-atmosphere system. These vectors provide a precise quantitative means of estimating and characterising the growth of small perturbations over a finite period of time under very general situations. Singular vectors have been used in two different ways. Following from the work of *Orr* (1907) in studying the transition to turbulence in Couette flow, these non-modal entities have been invoked to explain, for

example, laboratory fluid behaviour (e.g. *Trefethen et al*, 1993), extratropical cyclogenesis (e.g. *Farrell*, 1982), and even El Niño (*Penland and Sardeshmukh*, 1995). In the geophysical fluid dynamic context, let us refer to these as GFD studies.

However, singular vectors have also been shown to be intimately associated with the notion of predictability; specifically, with the estimation of the evolution of initial errors during the course of a forecast (*Lorenz*, 1965; Farrell, 1990). For example, *Molteni and Palmer* (1993) were able to explain, using singular vectors, the dependence of the weather forecast errors on the sign of the Pacific North/American mode. *Barkmeijer et al* (1993) have used localised singular vectors to quantify the predictability of short-range weather forecasts over Europe, and singular vectors are used routinely in the construction of the initial perturbations of the European Centre for Medium-Range Weather Forecasts ensemble prediction system (*Palmer et al*, 1993; *Molteni et al*, 1996; hereafter MBPP). A review of the role of singular vectors in predictability of the atmosphere and oceans from days to decades is given in *Palmer* (1996).

A third potential use of singular vectors is considered in this paper: in defining a strategy for utilising technology for making adaptive or targeted observations (principally) of the atmosphere. Such observations could be made, for example, from dropsondes released by unmanned aircraft pre-programmed to fly in dynamically-sensitive regions. The geographical location of such sensitive regions might vary from day to day, depending on actual and forecast atmospheric circulations. The quantitative location of such regions could be made from suitably-defined singular vectors. Such a strategy may be utilised in the FASTEX (Fronts and Atlantic Storm-Track Experiment) campaign (*Joly et al*, 1996; *Snyder*, 1996). In principle, adaptive observations could revolutionise the methodology for determining the initial conditions for weather prediction by coupling interactively the process of data assimilation and forecast with that of measurement.

Recently, *Buizza and Palmer* (1995; hereafter BP) have given a detailed account of the calculation of primitive equation atmospheric singular vectors in complete generality, i.e. for time-varying basic states, optimised for either global or localised energy growth. In BP, the essential non-modality of singular vector evolution was discussed, with emphasis on the upscale cascade of energy from sub-cyclone to cyclone scale, and the vertical propagation of energy from the baroclinic steering level to the upper tropospheric jet level. The methods and software used in BP form the basis of calculations in this paper.

In applying the singular vector technique for targeting observations, it is important to know whether the targeted observations are being made to study the precursors of the primary phenomenon (a GFD problem), or to improve the accuracy of initial conditions of a forecast of the primary phenomenon (a predictability problem).

The reason for making this distinction is that the inner product, or metric, with respect to which the singular vectors are computed, will be different depending on whether the calculations are being made for

GFD or predictability studies. With respect to the chosen metric, the singular vectors have unit amplitude at initial time, and evolve to have some maximal property at optimisation time. The dominant singular vector corresponds to the vector with largest amplitude at optimisation time, chosen from the set of all unit amplitude vectors at initial time. From a physical point of view, the appropriate metric is one for each of these unit amplitude vectors is equally likely, *a priori*. An important conclusion of this paper is that a unit vector which is likely from a purely GFD perspective, may be very unlikely from a predictability perspective. The reason for this difference lies in the fact that the predictability problem is constrained both by the observing network, and the process of assimilating and analysing the observations to produce the initial state. The GFD problem is not constrained in this way.

Hence, an important part of this paper is a discussion of the role of the metric in determining the structure of singular vectors. To do this, we use an index-based tensor formalism in which the role of the metric is explicit. This formalism is described in section 2. There is a purpose for not using the more conventional matrix notation. A difficulty of matrix notation is that the same object, the matrix, is used to represent different mathematical concepts, without distinction. For example, a generic matrix G might represent an operator (such as the tangent model) mapping vectors at initial time to vectors at final time. Alternatively G might represent products of two vectors (such as the covariance matrix of initial errors). Finally, G might also represent the inner product or metric mapping a pair vectors to the real line. This lack of distinction in conventional matrix notation can lead to obfuscation concerning metric dependency.

In section 3 examples of the dependence of singular vector structures on four simple choices of metric are discussed explicitly based on calculations made for growth optimised over a limited area relevant to FASTEX.

However, as discussed in section 4, there is, in principle, no arbitrariness in the choice of metric, for the application to the adative observation strategy. In section 5 we discuss which of the simple choices of metric defined in section 3 best approximates the predictability and GFD metric.

In addition to the singular vector methodology, two quite different techniques have been proposed for targeting adaptive observations: the breeding method (*Toth and Kalnay*, 1993, 1996) and potential vorticity (PV) diagnosis. An additional purpose of this paper is to compare the singular vector method with these two other techniques. These comparisons are performed in sections 6 and 7 respectively. For completeness, we discuss in section 8 a third proposal for targeting adaptive observations, the gradient sensitivity method. This is, in fact, closely related to the singular vector method.

In section 9 some specific practical examples for the use of singular vectors as a strategy for targeting potential adaptive observations in the pre-FASTEX period are made. Some remarks on their potential use for tropical cyclone and El Niño prediction are also made. A summary of results is made in section 10.

Throughout most of the paper, it is assumed that the dynamical system A is the midlatitude tropospheric circulation of the atmosphere. However, as mentioned above, in section 9 we consider the straightforward extension of the method to the coupled ocean-atmosphere system.

2. SINGULAR VECTOR FORMULATION

Consider an integration of A which generates a phase-space trajectory from an initial point X_0 to a forecast state X_1. The tangent propagator $L^i{}_j$ is a linear operator, mapping the tangent space T_{X_0} (i.e. the linear vector space of perturbations at X_0), to the tangent space T_{X_1}. That is to say, if $e^j \in T_{X_0}$ then

$$\hat{e}^i = L^i{}_j \, e^j \in T_{X_1}. \tag{1}$$

Now in (1), we have used an index-based tensor notation (e.g. *Dodson and Poston*, 1979) to denote vectors and linear operators. For example, using this notation, we distinguish between a vector e^i with its index "upstairs", and a covector, such as the gradient $\nabla_i J$, with its index "downstairs". Note that in (1), and elsewhere, the familiar "repeated-index" convention is used, whereby summation over all components is implied when the same index is repeated in a given multiplicative expression. Some justification for the use of this notation was given in the introduction to this paper.

In practice, for large numerical weather prediction models, the individual components of the tangent propagator are not known explicitly; rather $L^i{}_j$ is an operator given by a set of FORTRAN statements, which define a linearisation of the nonlinear model about a prescribed nonlinear solution (*Courtier et al*, 1991; BP).

We now define a metric g_{ij}, so that

$$d = g_{ij} \, e^i f^j \tag{2}$$

denotes the inner product between two arbitrary vectors e^i, f^i.

The inverse (or contra variant) metric g^{ij} can be defined by

$$g^{ij} g_{jk} = \delta^i{}_k \tag{3}$$

where $\delta^i{}_k$ is the Kronecker delta. In general, indices will be raised or lowered using these metric forms. Hence, for example, we can define the adjoint of the covariant form L_{ij} by

$$(L^*)_{ij} = L_{ji}. \tag{4}$$

Using (4), the operator form $(L^*)^i{}_j$ of the adjoint (the adjoint tangent propagator) can be expressed in terms of the metric forms and the forward tangent propagator by

$$(L^*)^i{}_j = g^{ik} g_{jl} L^l{}_k . \tag{5}$$

This operator maps the vector $\hat{e}^j \in T_{X_1}$ to the vector $(L^*)^i{}_j \hat{e}^j \in T_{X_0}$. The dependence of the adjoint propagator on the metric is explicit in (5).

Now eigenvectors of the compound operator

$$S^i{}_j = (L^*)^i{}_k L^k{}_j . \tag{6}$$

are precisely the singular vectors of $L^i{}_j$ in T_{X_0}, i.e. at initial time. The singular values σ are real and positive, and the singular vectors orthogonal (with respect to g_{ij}), since

$$S_{ij} = S_{ji} \tag{7}$$

even though for all realistic meteorological problems

$$L_{ij} \neq L_{ji} \tag{8}$$

The condition (8) has profound consequences for singular vector evolution as many authors have noted, following *Orr* (1907). One of the most important is that their evolution is not shape-preserving, i.e. non-modal (hence their description as optimal "modes" is not a good one). As discussed in BP, spectra of midlatitude singular vectors at initial and final time can show an upscale cascade and quantify what *Lorenz* (1993) refers to as the "butterfly effect".

In the singular vector calculation, the (primary) dynamical propagator can be multiplied with a further (secondary) operator $K^j{}_k$ to focus on specific aspects of perturbation growth. For example, *Barkmeijer et al* (1993) and BP have studied singular vectors optimised for localised areas. *Hartmann et al* (1995) have studied singular vectors optimised for different parts of the wavenumber spectrum. In these examples, the operator $K^j{}_k$ is a projection operator defined either in geographical or spectral space (equal to unity inside the targeted area, equal to zero outside). In the examples discussed here, we optimise total energy over the geographical domain D (30-80°N, 30°W-10°E).

(It is also possible to define a secondary projection operator $\tilde{K}^l{}_j$ at initial time. For example, consider an aircraft based at point p, with total range (out and return) of $2r$. Let $\tilde{K}^l{}_j$ be a projection operator equal to 1 for points inside the circle centred on p with radius r, and equal to zero for points elsewhere. Then with $K^i{}_k$ as above, the initial singular vectors of $K^i{}_k L^k{}_l \tilde{K}^l{}_j$ determine the structures within the range of the aircraft that are optimised over D at final time.)

The user is free to choose whatever secondary operator is felt to be most appropriate to the problem at hand. We have chosen to focus on the domain D because of the FASTEX experiment. Moreover, we have

chosen to optimise energy (as opposed, for example, to enstrophy) because winds and temperatures (rather than vorticity) are the primary variables that are used to validate weather forecasts, and hence measure their errors. However, it is important to stress that despite this there is, in principle, no choice in the metric g_{ij}. This is the subject of discussion in section 4-5.

In relation to its use for gradient sensitivity (e.g. *Cacuci*, 1981; *Rabier et al*, 1996; *Langland and Rohaly*, 1996), if we choose a scalar J, then the gradient $\nabla_i J \in T^*_{x_1}$ is transformed by the adjoint propagator and the metric to the sensitivity vector

$$s^i = (L^*)^i{}_j \, g^{jk} \, \nabla_k J \in T_{x_0}. \tag{9}$$

Note, from (5) and (9), that the sensitivity vector depends on the metric and on the scalar J. This is entirely analogous to the dependence of the singular vectors on the metric and the secondary operator (respectively). As with the secondary operator in the singular vector calculation, the choice of scalar J is arbitrary (e.g. it can be based on the variance of any chosen field; see section 8). However, we argue in section 4 below that, in principle, there is no freedom in the choice of metric.

3. DEPENDENCE OF SINGULAR VECTOR STRUCTURE ON CHOICE OF METRIC

As mentioned in the introduction, singular vectors have been calculated in a variety of contexts. In addition, a number of metrics have been used in the literature, e.g. based on enstrophy,

$$g^{(ENS)}_{ij} \, e^i f^j = \frac{1}{2} \int \zeta_{(e)} . \zeta_{(f)} \, dv ; \tag{10}$$

total energy,

$$\begin{aligned} g^{(ENE)}_{ij} \, e^i f^j = \frac{1}{2} \int & (\nabla \Delta^{-1} \zeta_{(e)} . \nabla \Delta^{-1} \zeta_{(f)} + \nabla \Delta^{-1} D_{(e)} . \nabla \Delta^{-1} D_{(f)} \\ & + R T_r \ln \pi_{(e)} . \ln \pi_{(f)} + \frac{C_p}{T_r} T_{(e)} . T_{(f)}) dv \end{aligned} \tag{11}$$

kinetic energy,

$$g^{(KE)}_{ij} \, e^i f^j = \frac{1}{2} \int \nabla \Delta^{-1} \zeta_{(e)} . \nabla \Delta^{-1} \zeta_{(f)} \, dv ; \tag{12}$$

or streamfunction variance

$$g^{(STR)}_{ij} \, e^i f^j = \frac{1}{2} \int \Delta^{-1} \zeta_{(e)} . \Delta^{-1} \zeta_{(f)} \, dv . \tag{13}$$

In (10)-(13), $\zeta_{(e)}$, $D_{(e)}$, $\pi_{(e)}$, $T_{(e)}$ represent, respectively, the vorticity, divergence, (log) surface pressure and temperature components of the vector e^i (similarly for f^i), and the integration is taken over the whole volume of the atmosphere. T_r is a reference temperature. The "dot product" in (10)-(13) denotes

the Euclidean inner product. Of course, the integral denotes a finite sum over all the (horizontal and vertical) components explicitly represented in the model.

In order to illustrate the impact of the choice of metric on the singular vector structure, singular vector calculations have been made using the ECMWF T42L19 tangent model based on a 48hour total energy optimisation within the target area D. The initial time is 12Z 5 December 1994. The circulation during this period was fairly zonal across the Atlantic, and not atypical of the sort of conditions that will be studied during FASTEX.

Fig 1 shows the streamfunction in the mid-troposphere (about 500hPa) of the dominant singular vector at initial time using a metric based on a) total energy, b) kinetic energy, c) enstrophy, d) streamfunction variance. Fig 2 shows the same field at optimisation time. In all cases, the contour interval at optimisation time is 20 times larger than at initial time. For the total energy singular vector (Fig 1a), the initial amplitude is fairly well localised over the west Atlantic, near the North American seaboard. Restricting the metric to kinetic energy (Fig 1b) has little impact on the structure of the dominant singular vector in terms of the mid-troposphere streamfunction, though growth rates are weaker. At initial time, the streamfunction of the kinetic energy metric is larger because unit kinetic energy norm is defined only in terms of the wind perturbations. The growth of the kinetic energy singular vector is weaker than the growth of the total energy singular vector because the initial temperature perturbations associated with the total energy metric play an important role in growth (see BP). However, the singular values of the dominant kinetic and total energy singular vectors, as measured in terms of their own metric, differ only by a factor of about 1.5; smaller than would be inferred from Figs 1 and 2 alone.

By contrast to results from either energy metric, the structure of the dominant enstrophy singular vector (Fig 1c) is fundamentally different, being dominated by planetary-scale perturbations. The structure of the dominant streamfunction singular vector (Fig 1d), on the other hand, has particularly small scale structure. Notice that, notwithstanding differences of scale, the maxima of either enstrophy or streamfunction singular vectors do not coincide with those of the energy singular vectors. Hence, if the maxima of the singular vectors were used as a criterion for targeting adaptive observations (cf section 9), the target regions would be metric dependent.

The final singular vectors, show, by construction, amplification over the target domain *D*. The principal maximum of the total energy singular vector (Fig 2a) is positioned close to the Greenwich meridian. Note that energy has propagated from the initial position at about 25-30 degrees per day, consistent with a typical Rossby wave group speed. For kinetic energy (Fig 2b) the final singular vector is very similar to that in Fig 2a. Despite its very different scale at initial time, the predominant scale of the enstrophy singular vector (Fig 2c) is similar to that of the energy singular vectors. There are differences, however. For example the centre over the eastern Atlantic is more prominent for the enstrophy singular vector, and, compared with the energy singular vectors, there is no high latitude component. The streamfunction singular vector at optimisation time is similar to the energy metric structures.

In Fig 3 the average energy spectrum of the first 16 singular vectors, computed with each of the energy, enstrophy and streamfunction metrics, is shown with respect to total wavenumber. The dashed lines show the spectrum at initial time, the solid lines show the spectrum at optimisation time. (From here on, kinetic energy singular vectors will not be shown explicitly as they are qualitatively similar, in terms of the diagnostics displayed in this paper, to those of total energy.) The initial spectra have been scaled by a variable factor to make them visible in the figure.

The spectrum of the energy singular vectors (Fig 3a) is fairly broad at the higher wavenumber half of the spectrum. The spectrum evolves with an inverse energy cascade peaking at cyclone scales. By contrast, the spectrum of the enstrophy-metric singular vectors peaks at low wavenumbers, and evolves by a energy cascade to cyclone scale and to higher wavenumbers (Fig b). Note that in Fig b there is no scaling between initial and final values; hence using the enstrophy metric, the singular vectors show virtually no energy growth, even though energy was being optimised at final time. This illustrates what a strong constraint the metric has on growth rates. Finally, the spectrum of the streamfunction-variance singular vectors (Fig c) is highly peaked towards very small scales (indeed it is peaked at the limit of truncation of the tangent propagator). As with the energy metric, there is an inverse cascade to larger scales. However, the scaling factor between initial and final time is an order of magnitude smaller than using the energy metric.

Fig 4 shows the vertical distribution of energy as a function of model level at initial (dashed) and final (solid) time, for the three choices of metric (and with scaling parameters between initial and final time as in Fig 3). For reference, level 7 corresponds to about 200 hPa, level 13 to about 700 hPa. It can be seen that for all choices, there is a tendency for an energy maximum in the mid to lower troposphere at initial time, with a maximum in the upper troposphere at final time. As discussed in BP, this is consistent with what would be expected from pseudomomentum conservation of wave activity. We defer further discussion of this issue to section 7.

4. THE COVARIANCE METRIC

We now introduce a probability function, or measure, μ . Specifically, $\mu(V)$ gives an *a priori* probability to a set $V \subset T_{x_0}$ of perturbations. In terms of μ we can address the question: " Are the perturbations V likely to occur?".

For the predictability problem, it is straightforward to define the appropriate measure μ_{pre} ; it gives the *a priori* probability that the actual initial error (considered as an element of T_{x_0}) is contained within V.

By contrast, given a perturbed set of phase-space points, generated by V and the "basic state" point p in phase space, the GFD measure $\mu_{GFD}(V)$ can be thought of as determining the probability that A's state vector lies in the set of perturbed points. For example, if all the perturbed points lie off A's attractor, then $\mu_{GFD}(V) = 0$. From a dynamical systems perspective, μ_{GFD} is determined from the invariant measure associated with the system's attractor in phase space (e.g. *Frisch*, 1995).

In general, whilst μ_{GFD} is only a function of the dynamics of A, μ_{pre} is, in addition, a function of the observing network and the data assimilation system used to create the initial state X_0. For example, from an empirical point of view, a very "approximate" attractor A_{dom} of the global atmospheric circulation could be defined from the dominant Empirical Orthogonal Functions (EOFs) of the global flow; from this empirical point of view, let $\mu_{GFD}(V) \approx 0$ if $V \not\subset A_{dom}$. However, there is no requirement that $\mu_{pre}(V) \approx 0$ for $V \not\subset A_{dom}$. To give an extreme example, suppose accurate observations of the atmosphere could be made (e.g. by advanced satellite soundings) on scales of 10km and greater, so that the source of cyclone-scale forecast inaccuracy would be associated with an upscale cascade of mesoscale initial error. We can suppose that atmospheric EOFs with scales of 10km or less do not contribute to A_{dom}. Hence if V denotes the set of perturbations with scales of 10km or less, then $\mu_{pre}(V) > 0$, $\mu_{GFD}(V) \approx 0$.

In general $\mu_{pre} \neq \mu_{GFD}$, as will be confirmed in section 5.

Now based on a given μ we can define the first and second moments

$$m^i = \int e^i d\mu, \tag{14}$$

$$C^{ij} = \int (e^i - m^i)(e^j - m^j)\, d\mu. \tag{15}$$

The integrand in (15) comprises the tensor product of pairs of vectors. Hence, from (1), C^{ij} is mapped to the forecast error covariance tensor

$$\hat{C}^{kl} = L^k{}_i L^l{}_j C^{ij}. \tag{16}$$

Note that $\hat{C}^{kl}$ is not itself metric dependent (which is not apparent from the equivalent matrix form $\hat{C} = LCL^*$, and the fact that the adjoint is metric dependent). However, let us make the specific choice of contravariant metric

$$g^{ij} = C^{ij} \tag{17}$$

then, from (5), (6) and (16)

$$\hat{C}^{ij} = S^{ij}. \tag{18}$$

Hence with the specific choice of contravariant metric (17), eigenvectors of $\hat{C}^i{}_j$ are precisely the evolved singular vectors of $L^i{}_j$. The vectors in T_{X_0} which evolve into these directions are the initial singular vectors of $L^i{}_j$.

Note, from (2) and (3), that the (covariant) form of the metric used to define the inner product between pairs of vectors is the inverse of the contravariant form, i.e.

$$g_{ij} = C^{-1}{}_{ij}. \tag{19}$$

In other contexts, the metric (19) is known as the Mahalanobis metric (e.g. *Mardia et al*, 1979); here we refer to the choice (19) as the covariance metric. For the predictability problem, the metric (19) will be referred to as the analysis error covariance metric (hereafter AECM). For GFD problems, the metric (19) is referred to as the GFD covariance metric (hereafter GFDCM).

The relationship between singular vectors and eigenvectors of the forecast error covariance tensor has also been discussed (in different forms) by *Houtekamer* (1995) and *Ehrendorfer and Tribbia* (1997).

It should be noted that, just as the AECM is the appropriate metric with which to define singular vectors for predictability studies, so also is it appropriate to define vectors which give the sensitivity of the forecast error to initial perturbations. From (9) and (17) , the AECM sensitivity vector is given by

$$s^i = (L^*)^i_{\ j}\ C^{jk}\ \nabla_k J. \tag{20}$$

We can interpret (20) as follows. Let J represent, for example, a rms forecast error, then s^i determines the sensitivity in forecast error with respect to perturbations drawn with respect to the probability distribution (associated with μ_{pre}) of initial analysis error.

5. RELATIONSHIP BETWEEN THE COVARIANCE AND OTHER METRICS

Overall results in section 3 show that there is a strong dependence of singular vector structure on the choice of metric. We now address the question as to which of the explicitly-estimated singular vectors gives the best approximation to the appropriate (AECM or GFDCM) covariance metric.

5.1 Evidence from analysis fields

For atmospheric predictability, the covariances of the initial or analysis error are not well known, and are not readily obtained from operational data assimilation schemes. However MBPP made an estimate of an analysis error field associated with one rather poor ECMWF forecast, by taking the difference between the ECMWF analysis and a corresponding DWD analysis, from which a hindcast (using the same ECMWF model) was much more successful. In this case one can assume that the difference between the ECMWF and DWD analyses was a fair estimate of the ECMWF analysis error.

In this paper, we extend this calculation by estimating the spectrum of a set of 42 difference fields produced from two sets of analyses: the operational ECMWF analysis, and an experimental analysis system that was being run in parallel at ECMWF at the time. It can be easily shown that if the two sets of analyses were each unbiased estimates of truth with uncorrelated error, then the variance of analysis difference fields would have the same spectral shape as the variance of analysis error fields. In practice it is unlikely that this condition is satisfied for these two analysis estimates, though the extent to which the condition is violated is hard to assess. (For example, it is possible that both sets of analyses have correlated deficiencies in their planetary-scale components.) For all cases in this set, the operational analysis system is based on the optimum interpolation (OI) scheme. For half of this set, the experimental

analyses were produced using the 3-dimensional variational data assimilation system (3DVAR; *Courtier et al*, 1993). For the other half, the OI scheme was used, though with a significant revision to the model formulation. The 42 cases were all taken from the northern winter.

Fig 5 shows the spectrum of the total energy, enstrophy and streamfunction squared averaged over all 42 difference fields. It can be seen that the energy spectrum is uniformly weighted over all wavenumbers. By contrast, that the enstrophy spectrum is strongly weighted towards high wavenumbers, whilst the streamfunction spectrum is strongly weighted towards low wavenumbers. These results are consistent with MBPP's single case study.

Now, by construction, the dominant AECM singular vectors must be contained in the subspace of eigenvectors of the analysis error covariance matrix. Hence, for a trial metric to be considered an approximation to the AECM, the spectra of the associated dominant singular vectors must not be inconsistent with the spectra of estimates of analysis error variance. Inconsistency is meant in the following sense: spectra of singular vectors are dominant in a wavenumber band for which the analysis error variance is relatively small. This inconsistency condition is clearly not sufficient to define the correct metric, since we do not address here questions relating to the horizontal and vertical correlation of errors. Nevertheless, the inconsistency condition is sufficient to distinguish between enstrophy, energy and streamfunction as choices of metric.

If energy, enstrophy and streamfunction variance are considered as candidate AECMs, only the energy metric satisfies our consistency condition. For example, as shown in Fig 3b, the initial structure of an enstrophy-based singular vector is essentially planetary scale, whilst Fig 5b shows that the enstrophy of the analysis difference fields is relatively negligible on planetary scales. Similarly, the initial structure of a streamfunction-based singular vector is essentially sub-cyclone scale (Fig 3c), whilst Fig 5c shows that the small scale streamfunction variance of the analysis difference fields is relatively negligible. For energy, in the range of wavenumbers in which the singular vectors have significant power, the analysis difference fields also have power (cf Figs 3a and 5a).

It is important to contrast the spectra of the difference fields with the spectra of the full analysis fields, which are shown in Fig 6. The full-field spectra are fundamentally different from those of the difference fields. In particular, both the energy and streamfunction spectra are peaked at low wavenumbers, whilst the enstrophy peaks at cyclone scales with a weak decay to high wavenumbers. The spectra of the full fields reflect the nonlinear structure of the atmospheric global circulation, and, in particular, the well-known QG enstrophy-cascading sub-range.

The fact that the energy spectrum of the analysis difference field is flatter than the energy spectrum of the analysis itself is entirely consistent with the process by which observations are utilised in a data assimilation scheme. As, for example, *Daley* (1985, 1991) and *Hollingsworth* (1987) have emphasised, observations necessarily constrain the low wavenumber components of the analysis more strongly than

the high wavenumber components. Hence, from a phase space perspective, not only will (good) observations ensure that the analysis error to have a smaller magnitude than the background error, they will cause the analysis error to rotate away from the background error towards smaller scales.

Whilst for the predictability problem, an energy-based metric appears to be the most suitable of those studied explicitly, it is clear from Fig 6 that it is not a consistent choice for GFD problems. In fact none of the simple choices of metric satisfy the consistency condition mentioned above. For example, as mentioned above, the dominant enstrophy singular vectors peak at low wavenumbers, where the analysis enstrophy spectrum shows relatively small amplitude. By contrast the streamfunction and energy singular vectors have most amplitude at sub-cyclone wavenumbers where the analysis amplitudes are relatively small.

However, one can define empirically a metric for which the singular vector spectra are not inconsistent (in the sense defined above) with the analysis variance spectra. In Fig 7, the dotted line shows the analysis enstrophy spectrum as in Fig 6. A piecewise linear function (shown as the dashed line) is fitted to this spectrum, and used to define the modified enstrophy metric $g^{(MOD\ \ ENS)}_{ij}$. The solid line in Fig 7 shows the spectrum of enstrophy defined with respect to this metric. To a first approximation, it is reasonably uniform across the wavenumber range (at least for cyclone-scale and higher wavenumbers).

Fig 8 shows the dominant singular vector using $g^{(MOD\ \ ENS)}_{ij}$ based, as above, for 48-hour optimisation in domain D at initial (5 December 1994) and final time. Compared with the enstrophy singular vectors, the scale of the modified enstrophy singular vectors is noticeably smaller (though not as small as the initial energy or streamfunction singular vectors). This is confirmed by analysing wavenumber spectra of the modified enstrophy singular vectors (not shown). At final time the singular vector structure is not dissimilar to those shown in Fig 2 for reasons discussed above. The metric $g^{(MOD\ \ ENS)}_{ij}$ is a crude empirical approximation to the GFDCM, having none of the correlation (or teleconnection) structures associated with the real atmosphere, nor indeed any vertical weighting. Nevertheless, the singular vector in Fig 8 is dependent, through the empirical construct $g^{(MOD\ \ ENS)}_{ij}$, on aspects of the nonlinear (quasi-turbulent) dynamics of the atmosphere, which determine the spectral characteristics of the atmosphere.

The vertical structure of the analyses difference fields and the full analysis fields, are shown in Figs 9 in terms of streamfunction variance. Once again, note that the structure of the difference fields is quite different from that of the full fields themselves; the full fields peak strongly in the upper troposphere whilst the difference fields are more uniformly distributed in the vertical. One possible explanation is that analysis differences in those circulation components generated by diabatic processes are comparable with errors associated with adiabatic advection. Since such diabatic processes influence the mid and lower troposphere more than the upper troposphere, this would tend to give a more uniform vertical distribution to the difference field. In addition, radiance observations from satellites, and wind observations from aircraft (which outnumber conventional radiosonde data) have a greater impact on the analyses in the upper troposphere.

5.2 Evidence from forecast error fields

The conclusion from section 5.1 was that the only of our candidate metrics to satisfy the consistency condition (for the analysis error variance) was energy. To give further support to this conclusion, results are shown in this section of the singular vector spectrum of forecast error, based on earlier calculations described in Barkmeijer et al (1993). The purpose of this is as follows: if we have chosen a good approximation to the AECM, then analysis errors will, on average, project uniformly onto all the initial singular vectors (i.e. the analysis error probability distribution will be isotropic in phase space). If this is true, then the projection of the forecast error onto the evolved singular vectors will be in proportion to the singular value itself.

To demonstrate this, 607 different 48hr operational ECMWF forecasts of 500hPa streamfunction for a chosen European region were projected onto 23 singular vectors computed from a T21L3 QG model (*Marshall and Molteni*, 1993) using a kinetic energy metric, and a secondary projection operator determined by the European region above. Results are shown in Fig 10. It can be seen that there is an excellent agreement between the magnitude of the projection of the forecast error onto the *i*th singular vector, and the *i*th singular value itself. In this case all of the variance of the forecast error can be explained by the projection onto these 23 singular vectors, about half of which are growing. This result supports the notion that the probability distribution of analysis error is approximately isotropic with respect to an energy-based metric. Similar results have been obtained for the hemispheric domain (*C. Reynolds*, personal communication, 1996).

5.3 The Hessian metric

Estimates of the AECM are possible in practice from variational data assimilation schemes (*Courtier et al*, 1993). Specifically, the Hessian of the variational analysis cost function J (the sum of background and observation cost functions) can be shown to be equal to the inverse of the analysis error covariance matrix (*Fisher and Courtier*, 1995). hence, the Hessian naturally defines a covariant AECM metric

$$g^{(VAR)}{}_{ij} = \nabla_i \nabla_j J \tag{21}$$

In practice, the resulting eigenvector equation for $S^i{}_j$ can be solved as a generalised eigenvector equation using a Jacobi-Davidson iterative solver (*Sleijpen and van der Vorst*, 1996).

Calculations of singular vectors using the 3DVAR hessian metric $g^{(3DVAR)}{}_{ij}$ are currently in progress. In 3DVAR, the background cost function involves the contraction of the first guess fields with (the inverse of) a fixed background covariance metric (*Courtier et al*, 1993). The formulation of this background metric involves a severe (and probably unrealistic) damping of the baroclinic scales (*Thépaut et al*, 1996), and at present, it is unclear whether use of the 3DVAR background metric is superior to the energy metric for singular vector calculations. A more satisfactory estimate of the flow-dependent background covariance matrix can, be obtained from the Kalman filter technique (*Fisher and Courtier*, 1995), which

propagates estimates of analysis error covariances using (16). Such a Kalman filter is currently under development at ECMWF (*F. Bouttier*, personal communication, 1996).

6 SINGULAR VECTORS AND BREEDING VECTORS

In this and the following two sections, we discuss three alternative strategies for adaptive observations: breeding vectors, potential vorticity diagnosis, and sensitivity vectors.

In the breeding method (*Toth and Kalnay*, 1993, 1996), a random perturbation is repeatedly evolved and rescaled to a specified amplitude over a relatively short cycling time, typically O (1 day), relative to an evolving nonlinear solution (let us call this the control integration trajectory). At any time, the bred perturbation can therefore obtained as the difference of two nonlinear integrations. In particular, no use is made of the tangent propagators at forecast time. Breeding vectors are used at NCEP as the basis of their ensemble forecasts. In addition, breeding vectors have been suggested as part of a possible strategy for adaptive observations (*Bishop and Toth*, 1996). In the linear limit the breeding vectors can be thought of as (quasi-) local Lyapunov vectors.

According to the philosophy of breeding, the breeding cycle mimics the analysis cycle. Let us break into this cycle and consider the first-guess error field at some given analysis time. The observations associated with that analysis time reduce (but do not necessarily wipe out) the amplitude of this first-guess error field, so that the analysis error also has significant projection onto the growing error carried forward by the first guess.

By contrast, according to the philosophy of singular vectors, the impact of observations in the analysis is to change the structure of the first-guess error, to the extent that the analysis error can have significant projection onto vectors which grow much faster than the local Lyapunov vector. This change in structure is believed to occur because the impact of data in the analysis is scale dependent; on large scales (e.g. cyclone scales), the analysis is strongly constrained by the observations, whilst on small scales (i.e. sub-cyclone scales) the analysis is relatively poorly constrained by the observations, and determined more by the background field (*Daley*, 1985, 1991; *Hollingsworth*, 1987). This change in structure, equivalent to a phase-space rotation towards small scales, will continually frustrate any tendency of the analysis error to asymptote towards the Lyapunov vector. Of course, in data sparse regions this phase-space rotation would be minimal. It might be argued that such regions occur over the oceans, and, in particular, over the North Atlantic where the FASTEX experiment is taking place. However, satellite, ship, buoy and aircraft data contribute substantially to the operational analyses over the North Atlantic (*Kelly et al*, 1993), and it would be simplistic to describe such regions as data sparse.

More generally, in comparing the realism of a given dominant breeding and singular vector, the following question is relevant. How does the growth rate of either vector compare with the projection of the analysis error onto that vector? If the dominant singular vector has an n-fold greater growth than the dominant breeding vector, then it will explain more of the forecast error, provided the projection of the analysis error

onto that singular vector is not less than n times that the projection of the analysis error onto the breeding vector.

Fig 11, shows an estimate of the growth of the first 200 breeding and (kinetic energy metric) singular vectors in the T21L3 quasi-geostrophic model of *Marshall and Molteni* (1993). Parameter values in the model are the same as in *Barkmeijer et al* (1993). Similar calculations of Lyapunov vector growth have been performed using this model by *Vannitsem and Nicolis* (1997).

In order to estimate the number of independent growing Lyapunov directions in the QG model, a set of 250 random orthogonal vectors has been constructed with non-dimensional kinetic energy of 10^{-10}. These have been used to create initial conditions for a 250 member ensemble. At the end of each 48-hour integration, the differences between the perturbed ensemble states and the unperturbed control integration have been orthonormalised with a Gram-Schmidt orthogonalisation, rescaling the amplitude to their initial value. This procedure is repeated over a large number (>400) of consecutive 48-hour periods. The solid line in Fig 11 shows the growth rate of the first 200 perturbations over a typical 48-hour period where the perturbations are ordered by the Gram-Schmidt procedure. It can be seen that the first orthogonal Lyapunov vector grows at a rate of 4 per 48 hour cycle time. The spectrum of growth rates decays rather slowly; the 100th breeding vector grows at a rate of about half the dominant breeding vector.

Singular vectors, optimised over the whole globe, were calculated over the same 48 hour period as the breeding vectors were estimated. The spectrum of singular values are shown as the dashed line in Fig 11. In contrast with singular vectors targeted over Europe, there are at least 200 growing directions, consistent with the breeding vector calculation. The dominant singular values are between 3 and 4 times those of the breeding vectors. Moreover, for the first 30 or so singular vectors, the spectrum of singular values decays much more rapidly than that of the breeding vectors. For example, the growth of the 10th singular vector is about half that of the dominant singular vector.

(It should be noted that these results are not consistent with a similar calculation performed by *Toth and Kalnay*, 1996, using a T10 model. In this latter set of calculations, the spectrum of dominant singular values has approximately the same slope as the spectrum of breeding vector growth rates. It is possible that the discrepancy can be explained by noting that the sub-cyclone to cyclone scale evolution of a characteristic energy metric extratropical singular vector cannot be simulated in a model with only T10 resolution.)

As mentioned above, in assessing the relative importance on atmospheric predictability of the dominant Lyapunov and singular vectors, one must also determine the relative projection of analysis error onto these vectors. If the energy metric were a good representation of the AECM, then these results suggest that more of the forecast error would be explained by the dominant singular vector than the dominant Lyapunov vector. However, this is clearly a contentious issue - and at present it must be concluded that both methods are viable as strategies for targeting adaptive observations.

Returning to Fig 11, it appears that, on a global basis, there are a substantial number of growing directions. However, when more local target areas are considered (using a secondary spatial projection operator), then the number of growing directions reduces in relation to the number of degrees of freedom in the target area. For example, as Fig 10 showed, the number of growing directions in the T21L3 quasi-geostrophic model for a 48-hour optimisation over a European region is about 10. This dramatic reduction in the number of growing directions for local domains is clearly relevant for the adaptive observation strategy: the smaller the domain that the observations are targeted for, the fewer the number of sensitive areas will be revealed by the singular vector calculation. For the FASTEX experiment, singular vector targeting is determined from the first four singular vectors (see section 9).

7 SINGULAR VECTORS AND POTENTIAL VORTICITY DIAGNOSIS

Potential vorticity has proven to be an extremely powerful diagnostic for analysing nonlinear advective processes in the atmosphere (e.g. associated with wave breaking; *McIntyre and Palmer*, 1984; *Hoskins et al*, 1985), and is now widely used to study atmospheric development. It has also been used as a tool for diagnosing the cause of forecast failure (e.g. *McIntyre*, 1988; *Appenzeller and Davies*, 1996). As such, PV diagnosis has also been proposed as a subjective technique for targeting the upstream observation component of FASTEX (*K. Browning, A. Thorpe*, personal communication).

In diagnosing PV development, it is common to focus on PV maxima on an isentropic surface which crosses the upper troposphere in midlatitudes. The Lagrangian velocity associated with the advection of such PV anomalies is quite unrelated to the group velocity of linear wave activity. For example, in the adiabatic approximation, air parcels are constrained to move on isentropic surfaces, whilst wave-activity can readily propagate through such surfaces. Insofar as the evolution of singular vectors tends to be readily describable in terms of wave-propagation effects, subjective PV targeting and singular vector analysis will not necessarily agree on the location of dynamically sensitive regions.

However, rather than argue from an idealised perspective, it is instructive to consider a particular case study. McIntyre (1988) has described a development occurring during 20-25 September 1982 where a tongue of high PV air breaks off from a stratospheric reservoir near Hudson bay, advects across the Atlantic, and rolls up to generate a surface cyclone. McIntyre hypothesises that a poor day-4 ECMWF forecast of this surface cyclone on 24 September may have resulted from small errors in the analysis of upper PV near the Hudson Bay area on 20 September. The 300K isentropic maps of PV for 20-25 September are shown in Fig 12.

In order to compare this PV-based estimate of sensitivity, dominant (energy metric) singular vector optimised for the region (50-60N, 10-20W) for 24 September 1982 (based on reanalysis initial conditions) are shown in Fig 13-14. Fig 13 shows the initial singular vector for a 48 hour optimisation, Fig 14 shows the initial singular vector for a 96 hour optimisation. For each optimisation time, we illustrate the singular vector at two different levels; at model level 9 (about 300hPa) and model level 15 (about 850hPa).

Let us first compare the initial singular vector structure for the 48 hour optimisation, valid for 22 September 1982. In the upper troposphere, the singular vector does not have a simple structure. However, most of the amplitude is concentrated between 70°-120°W and 40°-70°N. Insofar as it is possible to define a location with maximum amplitude, it appears to be at about 65°N, 70°W, which would correspond to a point on the western edge of the distorted PV anomaly for the 22nd, shown in Fig 12. However, the structure of the singular vector is better defined in the lower troposphere, where it suggests a localised wave train positioned right on the southern tip of the PV anomaly. Hence, in this case, there does appear to be some qualitative correspondence between the horizontal positions of sensitivity as suggested by PV and singular vector analyses, though there is some discrepancy as to what level in the atmosphere the forecast is most sensitive.

The initial singular vector for the 96-hour optimisation is valid for 20 September. (In practice, initial errors are likely to evolve nonlinearly over 4 days. However, we will ignore such complications here.) In the upper troposphere, the structure of the initial singular vector is rather indistinct, though the largest amplitudes are located in polar latitudes near 80°N, i.e. in the region of strong PV anomaly in Fig 12. However, in the lower troposphere there is again a more clearly-defined wavetrain structure close to 40°N and between 60° and 80°W, i.e. well south of the southernmost latitude of the PV anomaly for 20 September. Hence, whilst the 4-day singular vector structure suggests some sensitivity with respect to upper tropospheric perturbations of PV in polar latitudes, it also highlights an area of sensitivity both south of and lower in the atmosphere than would be apparent from the PV analysis.

The reason why the singular vectors have significant structure in the lower troposphere, whilst the PV-based sensitivity estimates do not, is consistent with difference between the dynamics of Lagrangian advection and wave propagation, as mentioned above. The (potential) enstrophy associated with wave activity propagating from the lower to upper troposphere (or from lower to higher latitudes) will amplify if the wave propagates from a region of small PV gradient into a region of strong PV gradient. This is dictated by pseudomomentum conservation (cf BP), a simple expression of which is given by the adiabatic frictionless form (e.g. *Andrews et al*, 1987)

$$\frac{1}{2}\frac{\partial}{\partial t}\left(\frac{\overline{q'^2}}{\bar{q}_y}\right) \quad \nabla . \boldsymbol{F} \quad 0 \tag{21}$$

for small amplitude Rossby waves propagating on a stationary zonally-symmetric basic state. Here, $\overline{q'^2}$ denotes wave potential enstrophy, $\bar{q}_y$ is the meridional gradient of basic state potential vorticity, and $\boldsymbol{F}$ is the Eliassen-Palm flux. The westward phase tilt of the initial singular vectors is consistent with a positive vertical component of the Eliassen-Palm flux, and hence upward propagation into the jet.

The lower tropospheric 4-day singular vector appears to be located in just such a region of weak PV gradient. Over the 4-day evolution period, the wave propagates both vertically and horizontally into the region of strong PV gradient in the upper troposphere over the target region. By contrast, for subjective PV targeting, the role of small PV anomalies in the lower troposphere (e.g. on 20 September) will tend

to be downplayed by the eye in comparison with the much larger PV anomalies in the region of strong gradient in the upper troposphere.

The crucial issue, as far as the relationship between these lower tropospheric singular vector structures and forecast sensitivity is concerned, is whether the component of analysis error in lower tropospheric (and lower latitude) PV anomalies projecting onto vertically-propagating waves, is large enough to be responsible for forecast errors in upper tropospheric PV. At present it is not possible to give a definitive answer to this. However, the answer does depends on the vertical distribution of variance in the AECM. As shown in Fig 9, the vertical distribution of variance associated with the (surrogate) analysis error fields is much broader than the distribution associated with the analyses themselves. The results in Fig 9 suggest that the *a priori* probability of an analysis error of given magnitude in the lower troposphere may not be so much different from the probability of an analysis error with the same magnitude in the upper troposphere. (Of course, these variance distributions do not prove that the initial error has sufficient projection onto vertically propagating modes to explain upper tropospheric forecast error.) As remarked above, possible explanations for these results could be the role of diabatic heating errors in the analysis, the relative accuracy of satellite sounding data in the upper troposphere, and the relative abundance of aircraft wind data in the upper troposphere.

It can be asked whether perturbations in lower tropospheric PV act as a trigger for upper tropospheric PV development, through pseudomomentum propagation. This is essentially a GFD question, rather than a predictability question. Compared with the analysis differences, the vertical distribution of streamfunction variance in the analysis is strongly weighted towards the upper troposphere (Fig 9). Conceivably this weighting (which would be implicit in the GFDCM) might be a sufficiently strong constraint as to eliminate these vertically-propagating waves in GFD singular vector computations in comparison with amplification by horizontal wave propagation in the upper troposphere. Such a calculation has not been performed.

8 SINGULAR VECTORS AND THE SENSITIVITY VECTOR

The third proposal (*Langland and Rohaly*, 1996) for a strategy for targeting adaptive observations is based on the sensitivity vector (9). In this proposal J is the lower tropospheric enstrophy of the forecast state. From a predictability perspective, this strategy can be thought of as targeting observations on the sensitivity of the component of forecast error that is correlated with the forecast state itself.

The sensitivity and singular vector methods are closely related. For example, if forecast error is expanded in terms of the (final-time) singular vectors, then the sensitivity vector can be written in terms of the initial singular vectors with coefficients of projection weighted by the singular values (*Rabier et al*, 1996).

In the limit where the secondary operator is a projection operator for a single model variable on a single gridpoint at a single level (i.e. there is only one degree of freedom left in the optimisation), then the initial singular vector and the sensitivity vector will agree precisely. One can anticipate that the sensitivity and singular vector methods will disagree more significantly when there are a number of singular vectors with comparable singular values. In this situation, the targeting domain based on the singular vector strategy may be more extensive than that based on the sensitivity analysis.

9 TARGETING PRODUCTS BASED ON SINGULAR VECTORS

Some examples of the use of the potential use of singular vectors to target observations have been given in Montani et al, 1996. In this section we show two examples of the use of singular vectors for targeting observations for the upstream component of FASTEX are shown in Fig 13, based on a the period immediately preceding the start of the FASTEX experiment (12Z 23 December 1996 and 12Z 30 December 1996). This period is of interest as the flow over the Atlantic region was rapidly developing (towards the establishment of a blocking anticyclone). The area shown covered with symbols denotes the region(s) over which aircraft dropsonde observations should be made, based on a set of the first 4 singular vectors optimised at 48 hours over the FASTEX intensive observing area. The calculations have been performed on a 48-hour forecast trajectory from T+24 to T+72 hours. In this way, the singular vector results can be disseminated in time for adequate flight preparation. For the FASTEX experiment, the choice of a 48 hour optimisation was considered desirable since on the one hand the most likely upstream targeting area would be easily within range of aircraft based on the east coast of the North American continent, and on the other hand, the optimisation period would not be so long as to jeopardise the assumption of linear error growth.

Specifically, the symbols denote regions where the amplitude of any of the first four singular vectors weighted by their respective singular value, exceeds 0.7 of the maximum amplitude of the dominant singular vector. This amplitude is calculated separately in terms of vorticity and temperature, though only the vorticity targets are shown in this paper.

For the first example shown (Fig 13a), the only targeted regions shown are associated with the dominant singular vector only. Moreover (not shown), the regions associated with maximum temperature and maximum vorticity roughly agree - indicating that the extra dropsonde observations should be made to the south of Newfoundland.

For the second example (Fig 13b), the targeted region is associated with an area over part of the UK and North Sea, well to the east of the FASTEX intensive observing area. The targeted region involves both the first and second singular vectors, but these roughly agree as far as the general geographical location of targeting is concerned.

These two examples show, for the same intensive observation area, how flow-dependent the targeted region can be. The reason the targeted region changes so much between the first and second dates can be explained in terms of the development of the strong blocking anticyclone over northern Europe and the western Atlantic during the last two weeks of December 1996.

In these examples, the singular vector calculations each indicate a relatively small targeting area. For other flow configurations there may be no single region. In fact for the date of the first example, 24-hour singular vectors did not indicate a single well-defined region: singular vectors 1 and 2 defining an area in the mid Atlantic, singular vectors 3 and 4 indicating a region over the UK itself (consistent with the developing blocking anticyclone, as mentioned above). In this situation it would not be possible to define a unique target region.

Although much of this paper has been motivated by the upstream component of FASTEX, there is a developing technology, described by *Holland et al* (1992) and *Langford and Emanuel* (1993) for which the singular vector targeting strategy could in principle be utilised on a more routine basis. The technology is based on the use of unmanned aircraft, which have been shown to be capable of flight to 100hPa with a range of many thousands of kilometres. Such aircraft could be capable of deploying a number of dropsondes during its flight. Autonomous navigation would be possible through the Global Positioning System, and data would be retrieved by satellite relay.

It should be noted that much of the original interest in unmanned aircraft was motivated by the tropical cyclone prediction problem (*Holland et al*, 1992; *Langford and Emanuel*, 1993). Singular vectors with moist physics included (e.g. *Vukicevic and Errico*, 1993; *Buizza et al* 1996; *J.F. Mahfouf*, personal communication), can, in principle, be used to target observations for tropical cyclones. Obviously, in this case, the secondary operator would not be fixed to a specific geographical area, but would be centred on the specific forecast tropical cyclone of interest.

Whilst all applications so far have been atmospheric, there is no reason in principle why singular vectors should not be used as a strategy for adaptive observations in the ocean. For example, *Chen et al* (1997) have calculated 6-month optimised singular vectors in an intermediate coupled ocean-atmosphere model of the tropical Pacific. In all situations studied, at initial time, the sea surface temperature of the coupled singular vector has a dipole structure oriented across the tropical Pacific basin in a north-west/south-east direction. The principal centre of action appears to be located close to, or just to the west of the dateline, varying in location by about 20 degrees of longitude depending on the season and state of El Niño in the basic state. An adaptive observation strategy making use of ship-based XBT measurements or maybe autonomous submarines, targeting the singular vector maximum in the west Pacific could be envisaged based on such analysis.

The next phase of research is to demonstrate the feasibility and impact of this strategy in data assimilation and forecast mode. Comparison of forecasts made from initial conditions with and without targeted

observations are required, though the impact of these forecasts should also be compared with forecasts made using randomly made extra observations. To some extent this could be done through (targeted) observation simulation experiments.

10 CONCLUSIONS AND SUMMARY

Singular vectors (of the linearised equations of motion) have been discussed in the scientific literature as a means of quantifying the growth of perturbations in the atmosphere and oceans, in order to explain the geophysical fluid dynamics of a particular climatic phenomenon (such as cyclogenesis or El Niño). Singular vectors have also been used to quantify how dynamically-active errors in forecast initial conditions evolve through the forecast. For this class of problem, the instability of the system, the specification of the network used to observe the system, and the process of assimilating the observations, are all relevant. In this paper, we discuss a third use of singular vectors: to define a strategy for targeting adaptive observations of the atmosphere (or the oceans). In such a strategy, observations would be made in particularly flow-dependent "sensitive" regions, determined by the location of the singular vectors at initial time. The developing unmanned aircraft technology could provide the practical means of realising such a strategy, though many of the calculations in this paper are motivated by the FASTEX experiment
.
In discussing their potential application as a strategy for targeting adaptive observations, it is important to decide whether the singular vector method is being applied in the GFD or predictability sense of the paragraph above. Such decision determines the most appropriate metric, or inner product, with which to compute the singular vectors. In order to make this metric dependence explicit, and to distinguish the mathematical objects used to define metrics, covariance matrices and tangent operators, an index-based tensor formalism is used in this paper to define the singular vectors and related quantities.

If the purpose of the targeted measurements is to improve the skill of forecasts of the primary phenomenon, then the singular vector metric should be consistent with the predictability measure μ_{pre} that gives the probability that an atmospheric state determined by a data assimilation system, corresponds to the true state of the atmosphere at the analysis time. By choosing a metric based on the second moment of the analysis error probability distribution, then the singular vectors at optimisation time are the eigenvectors of the forecast error covariance tensor. With respect to this metric (which we refer to as the analysis error covariance metric, AECM), the singular vector calculation is an optimisation taking into account the flow-dependent dynamical growth of any particular perturbation, constrained by the *a priori* probability that the analysis error might be described by that perturbation.

By contrast, if the purpose of the targeted observations is to study the precursors of the primary phenomenon, then the singular vector metric should be determined purely by the dynamical equations of motion alone. The appropriate probability measure μ_{GFD} and associated GFD covariance metric (GFDCM) will be given (in principle) by the invariant measure of the attractor determined solely by the dynamical equations of motion. In practice, the GFDCM could be obtained by a truncated EOF basis.

In this paper, energy, enstrophy and streamfunction variance were all considered as candidate metrics for singular vector calculations. From two independent sets of calculations based on analyses, and short range forecast data, it was shown that, of these three choices, energy is the most appropriate metric for the predictability problem. More accurate estimates of the AECM can in principle be obtained from variational and Kalman filter data assimilation technique.

Whilst the energy metric may be a reasonable first-order estimate of the AECM, it does not appear a suitable inner product for the GFD problem. A fundamental reason for this is that spectrum of analysis error appears to be relatively white (in terms of horizontal total wavenumber) compared with the equivalent spectrum of atmospheric variability (obtained from the analysis fields themselves). With an energy inner product, initial singular vector structures are predominantly sub-cyclone scale, which is consistent with the spectra of analysis error, but not with the spectra of the analyses themselves.

The reason why the analysis error spectra appear to be whiter than the spectra of the analyses themselves is basic to the methodology of data assimilation. In data assimilation, the observations are added to a background field, itself a forecast field from an earlier initial analysis. However, the impact of such observations are scale dependent, constraining the larger scales (well resolved by the observing network) much more strongly than the smaller scales. Hence the role of observations is to damp preferentially the amplitude of background forecast error at low wavenumbers, and hence to generate a whiter analysis error spectrum than the background error spectrum.

For FASTEX, the main purpose of the targeted observations is to improve the predictive skill of forecasts for the intensive observation area over the eastern Atlantic. Examples of products produced in the pre-FASTEX period are shown based on the first four energy metric singular vectors, optimised for the intensive observation area.

In addition to singular vectors, three other techniques have been proposed for adaptive observation strategies: the breeding method, subjective potential vorticity analysis and sensitivity analysis. These additional methods were compared with the singular vector strategy. With the exception of sensitivity analysis, which is also a metric-dependent adjoint method, these methods can generate quite different regions for observation targeting from that associated with the singular vector method.

Reasons for these differences are discussed in the body of the paper. Differences between breeding and singular vectors reflect the differences between Lyapunov and optimal growth. Their relevance to targeting for predictability depends on the growth rates of these vectors, and on their projection onto analysis error. Discrepancies in targeting based on singular vectors and PV analysis can be explained in terms of the different perspectives associated with Lagrangian advection and wave propagation. For the latter, pseudomomentum conservation can lead to regions of sensitivity being located in areas of weak PV gradient.

Ultimately an assessment of the optimal strategy for observation targeting can only be assessed by comparing the impact of extra observations made using each of the candidate strategies, on forecast skill.

ACKNOWLEDGEMENTS

Our thanks to P. Courtier, R. Daley, K. Emanuel, A. Hollingsworth, P. Ioannou, A. Joly, E. Kalnay, A. Persson, A. Simmons, C. Snyder, D. Stephenson, A. Thorpe, and Z. Toth for many helpful comments and discussions. We thank A. Montani of Reading University for producing Fig 15.

REFERENCES

Andrews, D.G., Holton, J.R. and Leovy, C.B., 1987: *Middle Atmosphere Dynamics.* Academic Press. 489pp.

Appenzeller, Ch., Davies, H.C., Popovic, J. M., Nickovic, S., Gavrilov., M.B., 1996: PV morphology of a frontal-wave development. *Meteorology and Atmospheric Physics*, 58, 21-40.

Barkmeijer, J., P. Houtekamer and Xueli Wang, 1993: Validation of a skill prediction method. *Tellus*, 45A, 424-434.

Bishop, C. H. and Z. Toth, 1996: Using ensembles to identify observations likely to improve forecasts. Preprints, 11th AMS Conference on Numerical Weather Prediction, Norfolk, Virginia, p. 72-74.

Buizza, R. and T.N. Palmer, 1995: The singular vector structure of the atmospheric general circulation. *J.Atmos.Sci.*, 52, 1434-1456.

Buizza, R., T.N.Palmer, J.Barkmeijer, R. Gelaro and J.F. Mahfouf, 1996: Singular vectors, norms and large-scale condensation. Preprints, 11th AMS Conference on Numerical Weather Prediction, Norfolk, Virginia, p. 50-51.

Cacuci, D.G., 1981: Sensitivity theory for nonlinear systems. I: Nonlinear functional analysis approach. *J. Math. Phys.*, 22, 2794-2802.

Chen, Ying-Quei, D.S. Battisti, T.N. Palmer, Joseph Barsugli, and E.S. Sarachik, 1997: A study of the predictability of tropical Pacific SST in a coupled atmosphere-ocean model using singular vector analysis: the role of the annual cycle and the ENSO cycle. *Mon. Wea. Rev.*, 125, 224-238.

Courtier, P., C. Freydier, J.-F. Geleyn, F. Rabier and M. Rochas, 1991: The Arpege project at Meteo-France. Proceedings of ECMWF seminar on "*Numerical methods in atmospheric models*". Vol2, p 193-231. ECMWF, Shinfield Park, Reading, RG2 9AX, UK.

Courtier, P., E.Andersson, W.Heckley, G.Kelly, J.Pailleux, F.Rabier, J.N. Thepaut, P. Unden, D.Vasiljevic, C.Cardinali, J.Eyre, M.Hamrud, J.Haseler, A.Hollingsworth, A.McNally, A.Stofflen, 1993: Variational Assimilation at ECMWF. ECMWF Research Department Technical Memorandum 194. ECMWF, Shinfield Park, Reading, RG2 9AX, UK.

Daley, R., 1985: The analysis of synoptic scale divergence by a statistical interpolation scheme. *Mon.Wea.Rev.*, 113, 1066-1079.

Daley, R., 1991: Atmospheric Data Analysis. Cambridge University Press. pp457.

Dodson C.T.J. and T. Poston, 1979: *Tensor Geometry*. Pitman Publishing. pp598.

Ehrendorfer, M. and J.J.Tribbia, 1997: Optimal prediction of forecast error covariances through singular vectors. *J.Atmos.Sci.*, 53, 286-313.

Farrell, B.F., 1982: The growth of disturbances in a barolinic flow. *J.Atmos.Sci.*, 39, 1663-1686.

Farrell, B.F., 1990: Small error dynamics and the predictability of atmospheric flows. *J.Atmos.Sci.*, 46, 1193-1206.

Fisher, M. and P. Courtier, 1995: Estimating the covariance matrices of analysis and forecast error in variational data assimilation. ECMWF Research Department Technical Memorandum No. 220. ECMWF, Shinfield Park, Reading, RG2 9AX, UK.

Frisch, U., 1995: *Turbulence*. Cambridge University Press. pp296.

Hartmann, D.L., R. Buizza and T.N.Palmer, 1995: Singular vectors: the effect of spatial scale on linear growth of disturbances. *J.Atmos.Sci.*, 52, 3885-3894.

Holland, G.J., T. McGeer and H.Youngren, 1992: Autonomous aerosondes for economical atmospheric soundings anywhere on the globe. *Bull. Amer. Meteor. Soc.*, 73, 1987-1998.

Hollingsworth, A., 1987: Objective analysis for numerical weather prediction. In: Short and Medium Range Numerical Weather Prediction. Collected papers presented at WMO/IUGG NWP symposium, Tokyo, 4-8 August, 1986, ed T.Matsuno, Special volume of the *J.Meteor.Soc.Japan.*, 11, 59.

Hoskins, B.J., M.E.McIntyre and A.W.Robertson, 1985: On the use and significance of isentropic potential vorticity maps. *Q.J.R.Meteor.Soc.*, 111, 877-946.

Houtekamer, P.L., 1995: The construction of optimal perturbations. *Mon.Wea.Rev.*, 123, 2888-2898.

Joly, A., D.Jorgensen, M.A.Shapiro, A.Thorpe, P.Bessemoulin, K.A.Browning, J.-P. Cammas, J.-P. Chalon, S.A.Clough, K.A.Emanuel, L.Eymard, R.Gall, P.H.Hildebrand, R.H.Langland, Y.Lemaître, P.Lynch, J.A.Moore, P.O.G. Persson. C. Snyder, R.M.Wakimoto, 1996: The Fronts and Atlantic Storm-Track Experiment (FASTEX): Scientific Objectives and Experimental Design. Report Number 6. The FASTEX Project Office, Météo-France, CNRM, 42 Avenue Coriolis, Toulouse, France. (Also submitted to Bull. Am. Met. Soc.).

Kelly, G., J. Pailleux, F. Rabier and J.-N. Thépaut, 1993. Observing system experiments made with the ECMWF system. World Weather Watch Technical Report No. 16, WMO/TD No 594. World Meteorological Organisation. Geneva.

Langford, J.S. and K.A.Emanuel, 1993: An unmanned aircraft for dropwindsonde deployment and hurricane research. *Bull. Amer. Meteor. Soc.*, 74, 367-375.

Langland, R.H. and G.D.Rohaly, 1996: Adjoint-based targeting of observations for FASTEX cyclones. Proceedings of Seventh AMS Mesoscale Processes Conference. American Meteorological Society.

Lorenz, E.N., 1965: A study of the predictability of a 28-variable atmospheric model. *Tellus*, 17, 321-333.

Lorenz, E.N., 1993: *The essence of chaos*. University of Washington Press. Seattle, USA. pp 227.

Mardia, K.V., J.T. Kent and J.M. Bibby, 1979: *Multivariate analysis.* Academic Press. 518pp.

Marshall, J and Molteni, F., 1993: Towards a dynamical understanding of planetary-scale flow regimes. *J.Atmos.Sci.*, 50, 1792-1818.

McIntyre, M.E. and T.N.Palmer, 1984: The "surf zone" in the stratosphere. *J.Atmos.Terr. Phys.*, 46, 825-849.

McIntyre, M.E., 1988: The use of potential vorticity and low-level temperature/moisture to understand extratropical cyclogenesis. ECMWF 1987 Seminar Proceedings Vol 1. ECMWF, Shinfield Park, Reading, RG2 9AX, UK.

Molteni, F. and T.N.Palmer, 1993. Predictability and finite-time instability of the northern winter circulation. *Q.J.R.Meteorol.Soc.*, 119, 269-298.

Molteni, F., R. Buizza, T.N.Palmer and T.Petroliagis, 1996: The ECMWF ensemble prediction system: methodology and validation. *Q.J.R.Meteorol.Soc.*, 122, 73-120.

Montani, A., R. Buizza and A.J.Thorpe, 1996: Singular vector calculations for cases of cyclogenesis in the north Atlantic storm-track. Preprints, 7th AMS conference on mesoscale processes. p 391-392.

Orr, W. Mc F., 1907: Stability or instability of the steady motions of a perfect liquid. *Proc.Roy. Irish Acad.*, 27, 9-69.

Palmer, T.N., F. Molteni, R. Mureau, R. Buizza P.Chapelet, and J. Tribbia, 1993: *Ensemble prediction.* ECMWF Seminar proceedings on Validation of models over Europe Vol 1, ECMWF, Shinfield Park, Reading, RG2 9AX, UK.

Palmer, T.N., 1996: Predictability of the atmosphere and oceans: from days to decades. In "*Decadal climate variability - dynamics and predictability*", NATO ASI Series, Subseries I "Global Environmental Change", Vol. 44, ed D.Anderson and J. Willebrand. pp83-155. Springer.

Penland, C. and Sardeshmukh, P.D., 1995: The optimal growth of tropical sea surface temperatures. *J.Climate*, 8, 1999-2024.

Rabier, F., E. Klinker, P.Courtier and A. Hollingsworth, 1996: Sensitivity of forecast errors to initial conditions. *Q.J.R.Meteorol.Soc.*, 122, 121-150.

Sleijpen, G.L.G. and H.A. Van der Vorst, 1996: A Jacobi-Davidson iteration method for linear eigenvalue problems. *SIAM J. Matrix Anal.Appl.*, 17, 401-425.

Snyder, C., 1996: Summary of an informal workshop on adaptive observations and FASTEX. *Bull. Am. Met. Soc.*, 77, 953-961.

Thépaut, J.N., P.Courtier, G.Belaud and G.Lemaître, 1996: Dynamical structure functions in a four-dimensional variational assimilation. A case study. *Q. J.R.Meteorol.Soc.*, 122, 535-562.

Toth, Z. and E. Kalnay, 1993: Ensemble forecasting at NMC: the generation of perturbations. *Bull.Amer.Meteor.Soc.*, 74, 2317-2330.

Toth, Z. and E.Kalnay, 1996: Ensemble forecasting at NCEP. ECMWF seminar on "*Predictability*" vol II. ECMWF. Shinfield Park, Reading, RG2 9AX, UK. pp259.

Trefethen, L.N., A.E.Trefethen, S.C.Reddy and T.A.Driscoll, 1993: Hydrodynamic stability without eigenvalues. *Science*, 261, 578-584.

Vannitsem, S. and C. Nicolis, 1997: Lyapunov vectors and error growth patterns in a T21L3 quasi-geostrophic model. *J.Atmos.Sci.*, 54, 347 - 361.

Vukicevic, T. and R.M. Errico, 1993: Linearization and adjoint of parametrized moist diabatic processes. *Tellus*, 45A, 493-510.

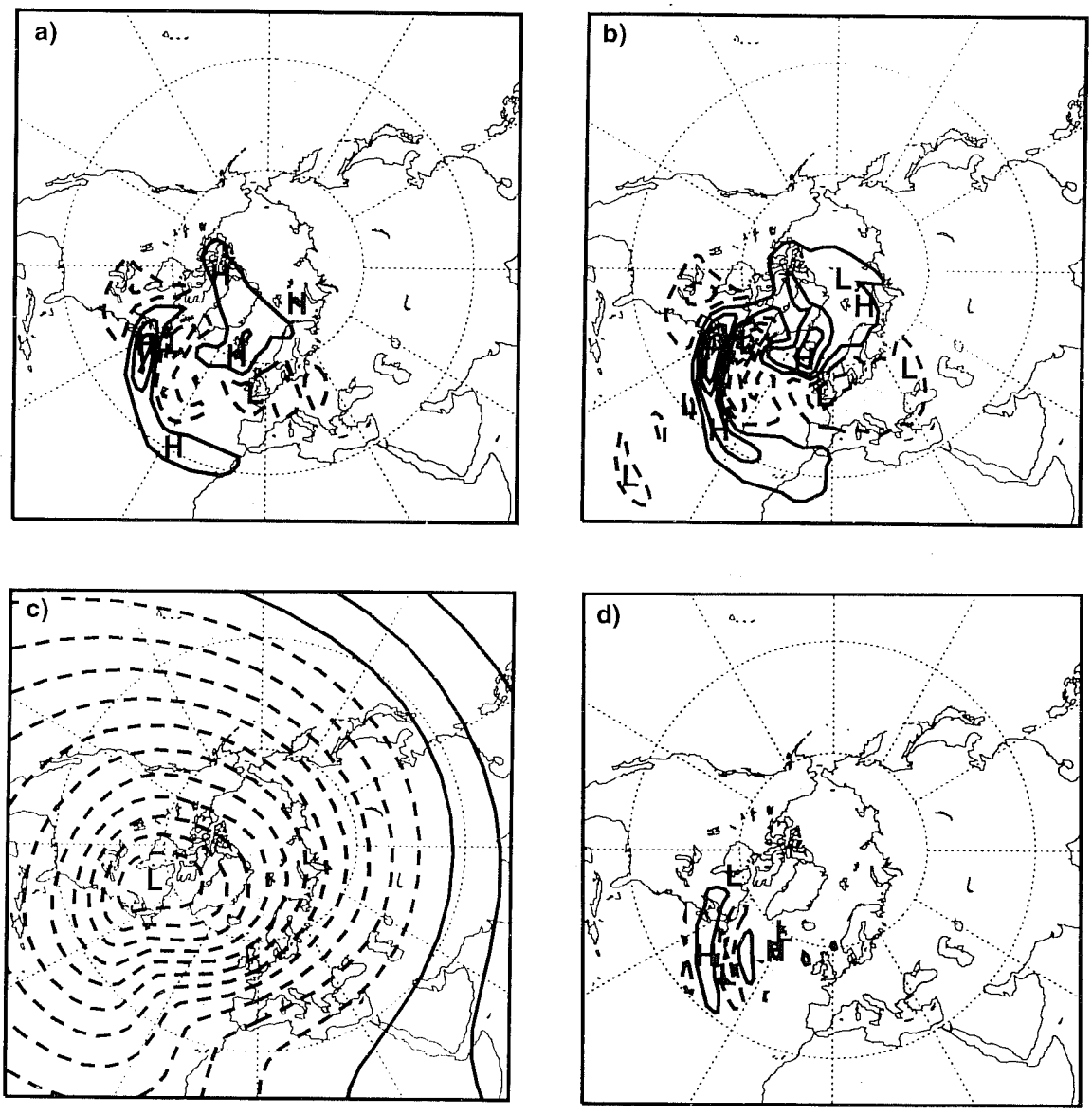

Fig. 1 Streamfunction of dominant 48-hour singular vector on a model level near 500hPa optimised for energy growth in the target area 30-80N, 30W-10E at initial time. Initial date 12Z 5 December 1994. Metric used: a) total energy, b) kinetic energy, c) enstrophy, d) streamfunction variance. See Fig 2 caption for information about contour intervals.

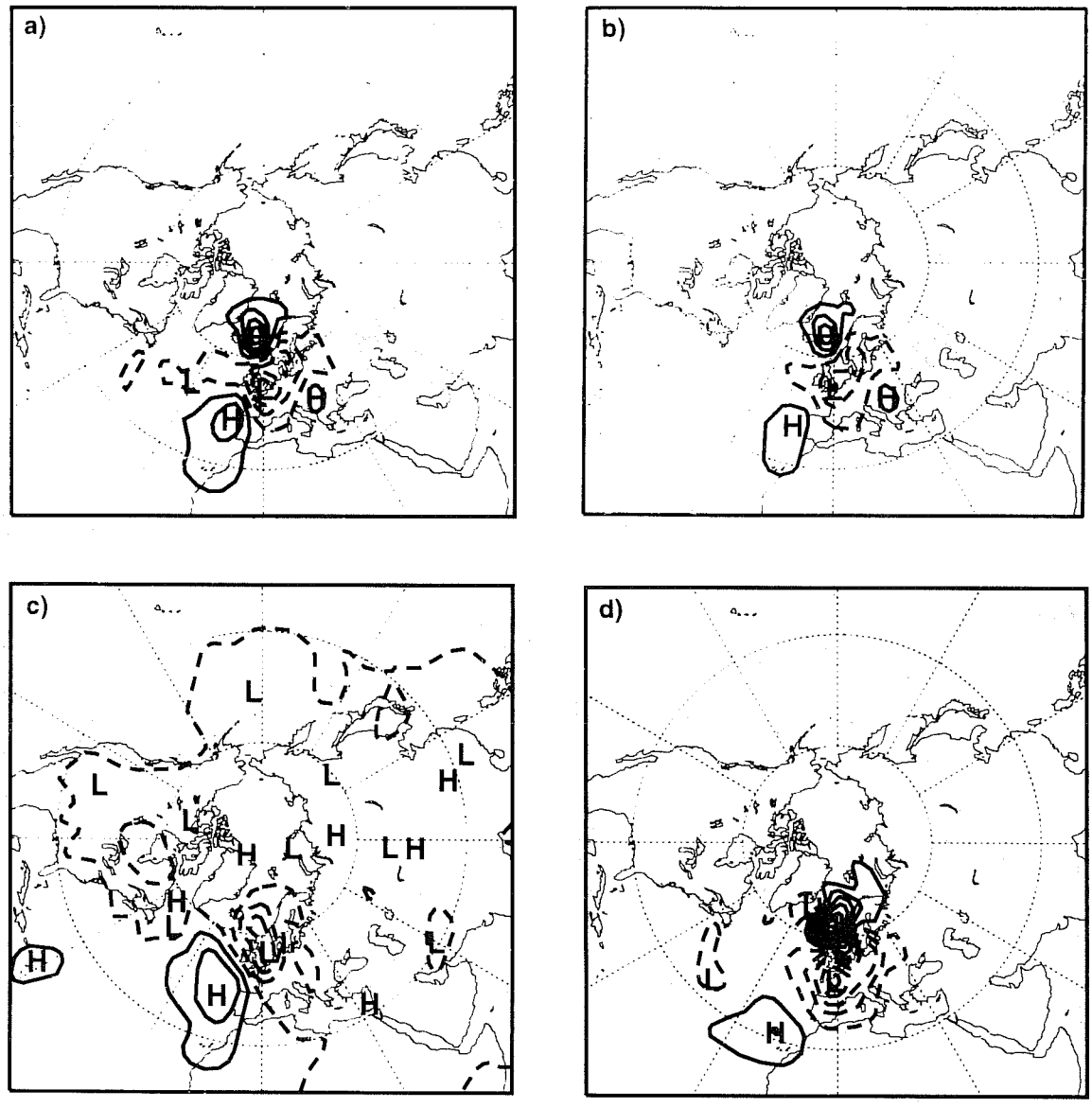

Fig. 2 As Fig 1, but at optimisation time. For each of a)-d), the contour interval is 20 times larger than in the corresponding component of Fig 1.

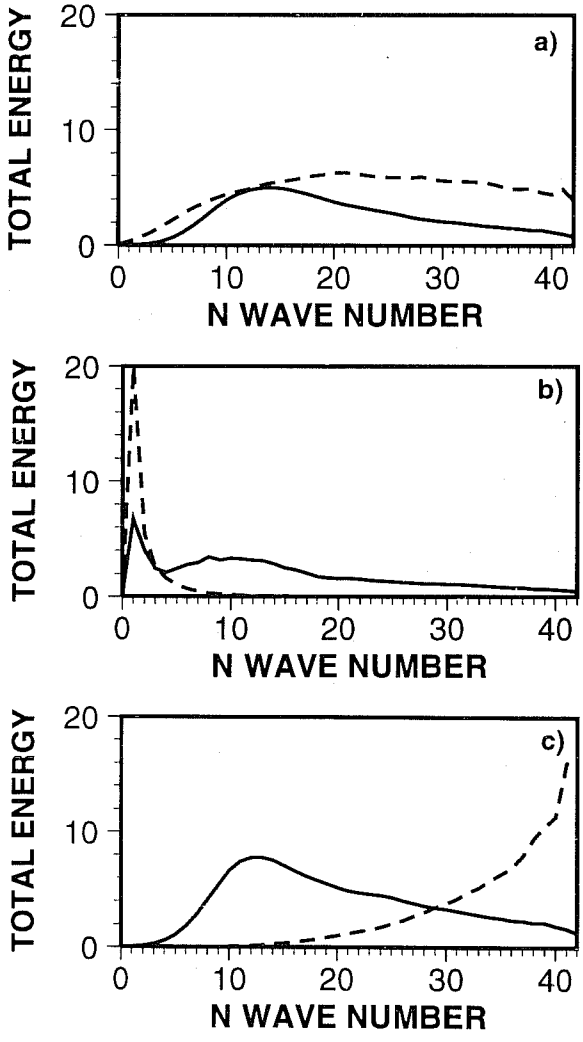

Fig. 3 Energy specrum of first 16 singular vectors (as a function of 2D total wavenumber) computed using optimisation and iinitial conditions as in Fig 1, and 2. a) total energy, b) enstrophy, c) streamfunction variance. Dashed line shows spectrum at initial time, solid line shows spectrum at optimisation time. The spectra at final time have been reduced by the following factors (so that initial and final spectra can be plotted together): a) 100, b) 1, c) 10.

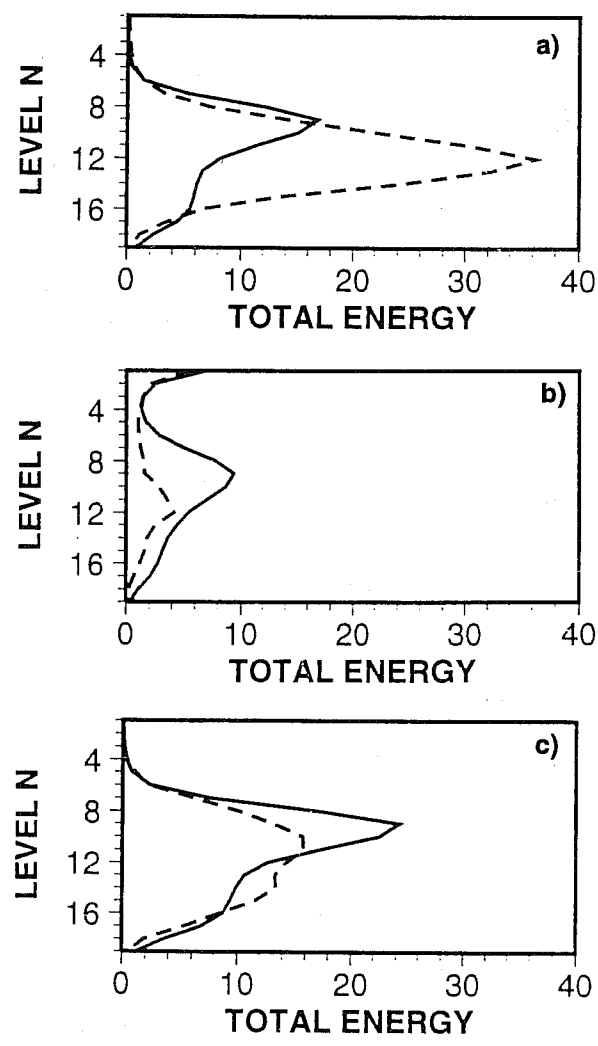

Fig. 4 The vertical distribution of energy averaged over the first 16 singular vectors (as in Fig 3) at initial (dashed) and optimisation (solid) time. The distributions at final time have been reduced by the following factors (so that initial and final distributions can be plotted together): a) 100, b) 1, c) 10.

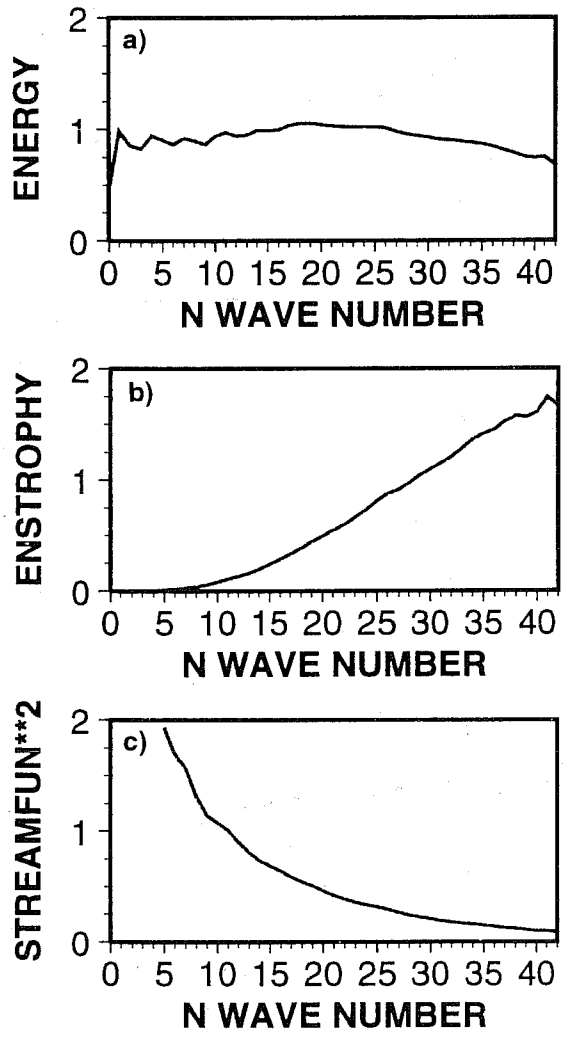

Fig. 5 Spectrum of the variance of a set of 42 analysis difference fields as a function of total wavenumber based on: a) total energy, b) enstrophy c) streamfunction variance. Each field is the difference between two quasi-independent analyses for the same date. The curves have each been scaled by a suitable factor to make them mutually comparable.

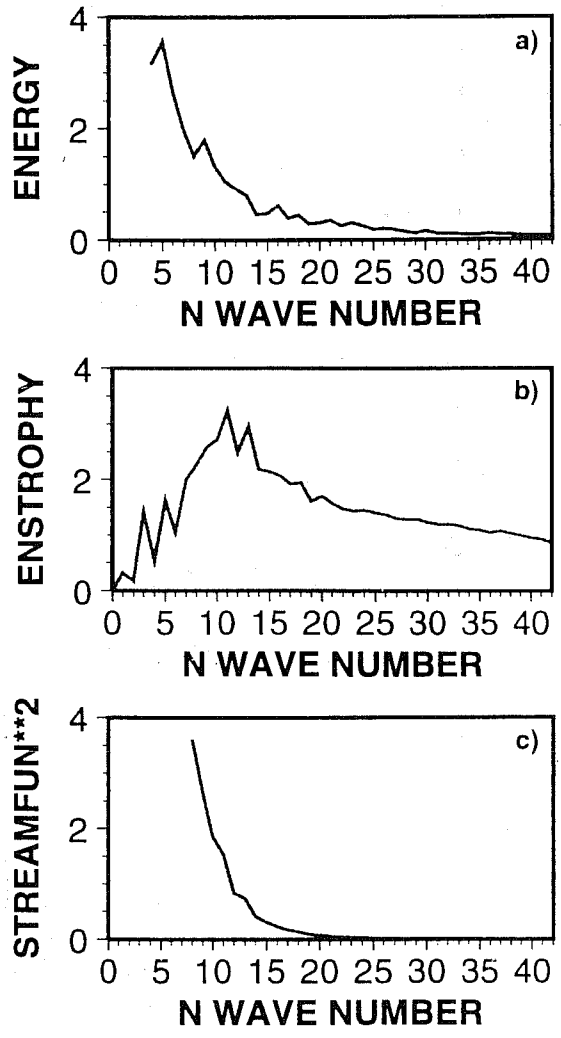

Fig. 6 As Fig 5, but for the full analysis fields.

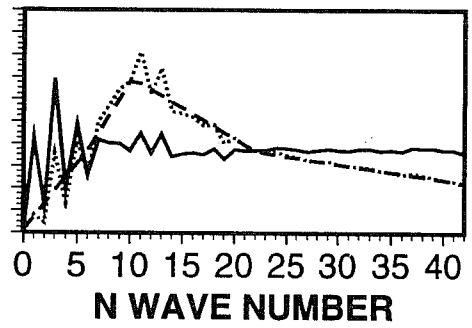

Fig. 7 Enstrophy spectrum from full analysis fields (dotted). Piecewise linear fit to enstrophy spectrum (dashed). Modified-enstrophy spectrum (solid) based on the amplitude of the vorticity fields using a modified enstrophy metric defined from the dashed line.

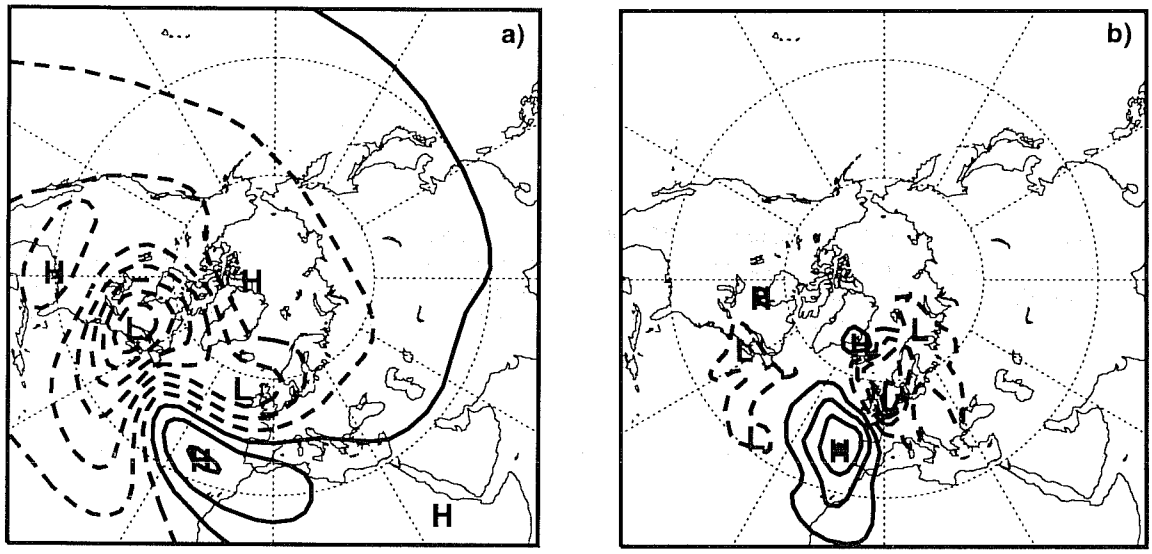

Fig. 8 a) Initial singular vector, as Fig 1 c, but using the modified enstrophy metric. b) Singular vector at optimisation time, as Fig 2c, but using the modified enstrophy metric. The contour interval at final time is 20 times larger than at initial time.

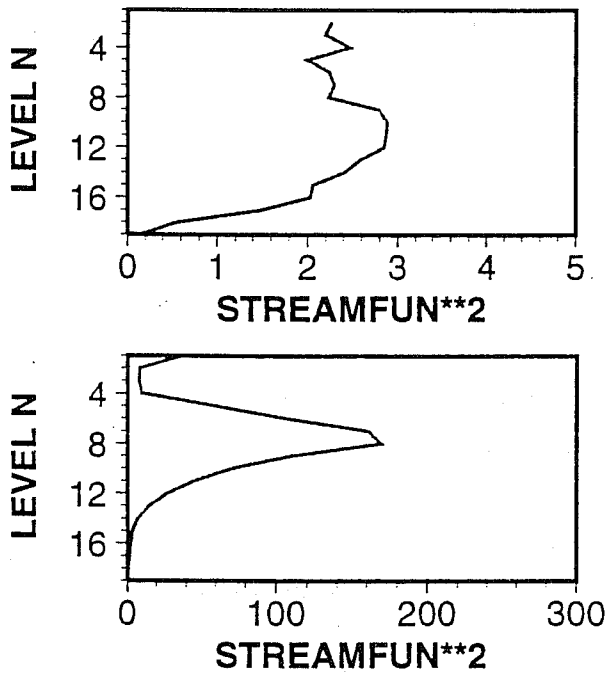

Fig. 9 Streamfunction variance of a) the analysis difference fields b) the full analysis fields, as a function of model level.

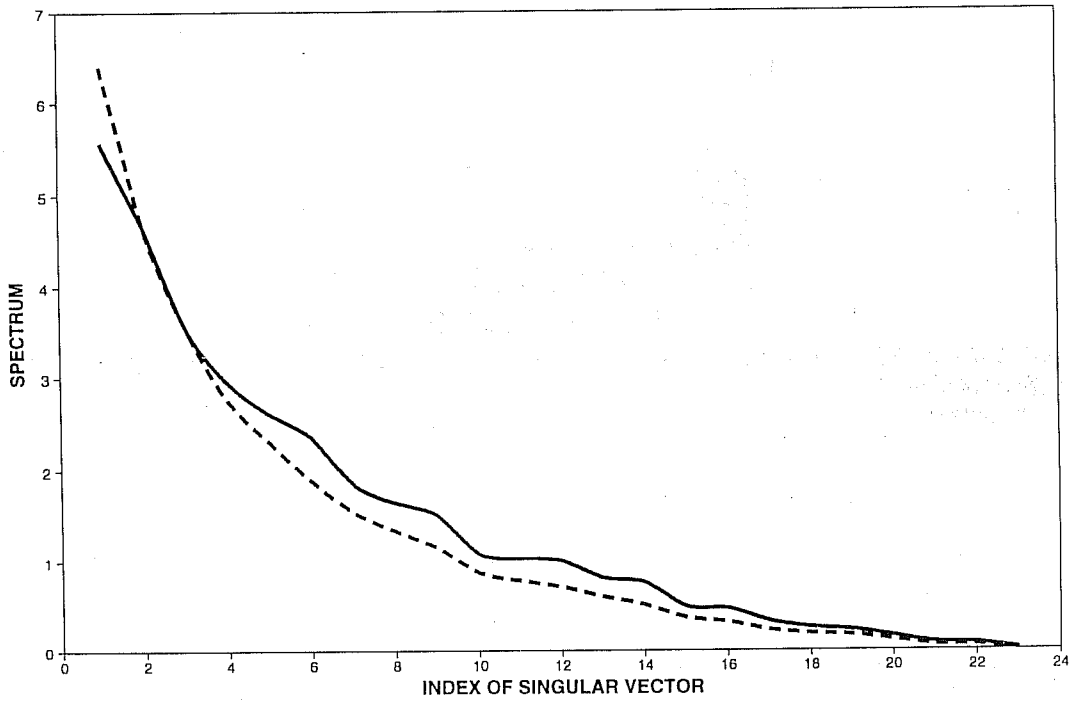

Fig. 10 Solid line: the mean projection of the 2-day ECMWF forecast error for western Europe, projected onto the appropriate 2-day kinetic-energy singular vectors, for 607 separate forecasts. The percentage of explained forecast error variance associated with a particular singular vector is given by the square of the ordinate value of the solid line. Dashed line: the normalised mean singular value spectrum for those 607 days. Further details are given in Barkmeijer et al (1993).

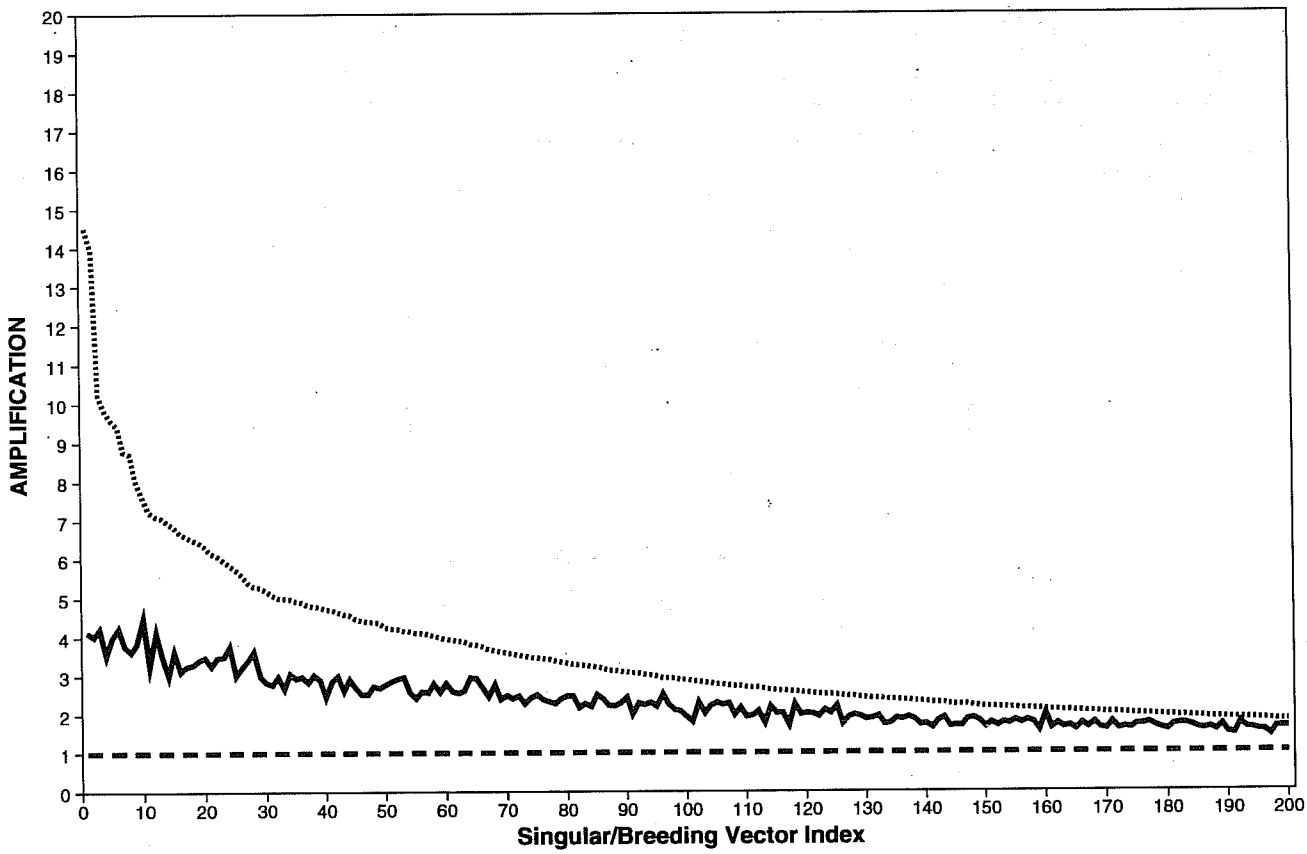

Fig. 11 Solid line: the growth of orthogonal Lyapunov vectors over a typical 48-hour period from the QG model. Heavier dashed line: singular values over the same 48-hour period. The neutral growth line is also shown for reference.

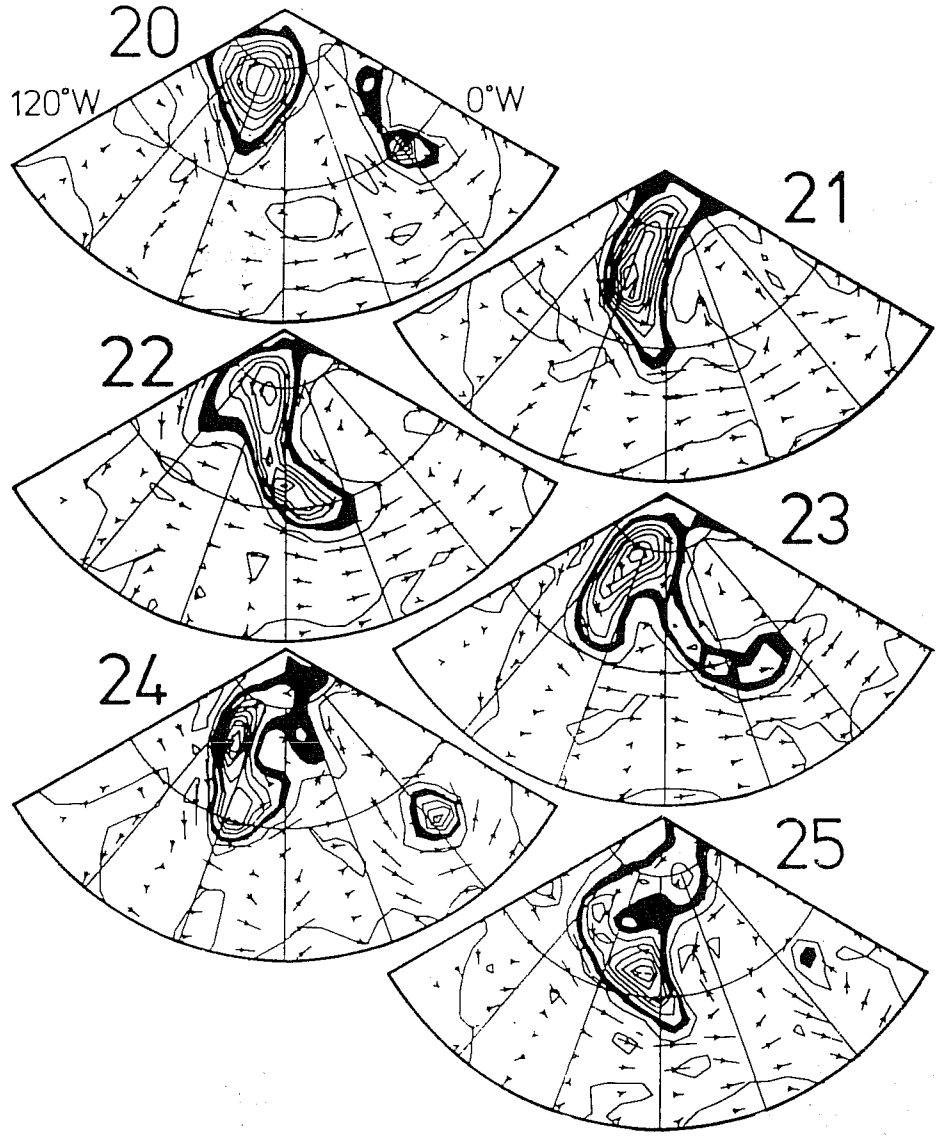

Fig. 12 300K isentropic maps of PV for 20-25 September 1982, from ECMWF operational analyses. Latitude circles are 40N, 60N, and 80N; Greenwich meridian on the right, 120W on the left. See Mcintyre (1 988) for details.

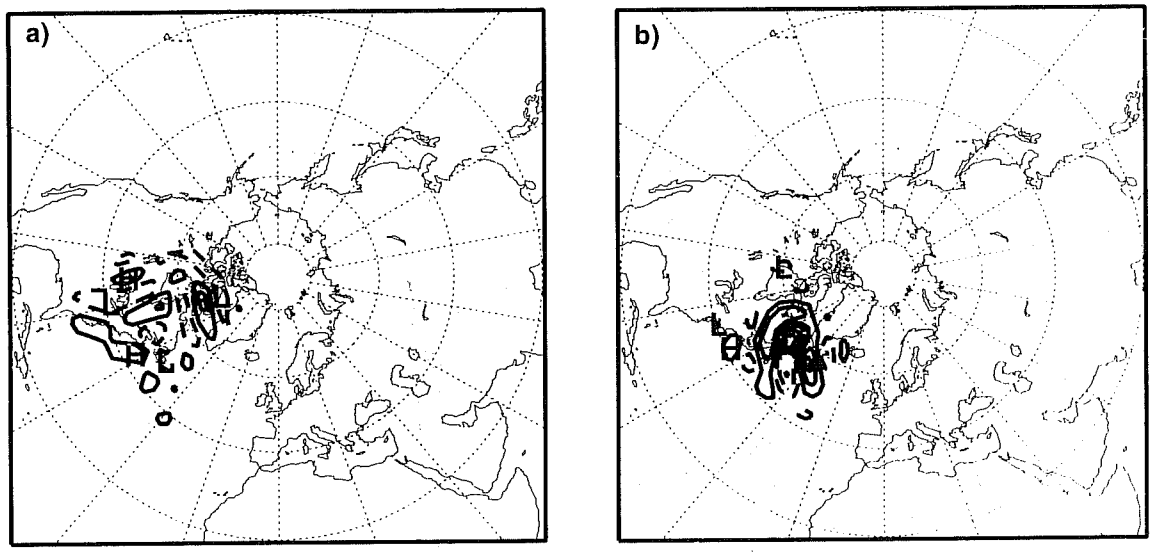

Fig. 13 Streamfunction for initial 48-hour singular vector optimised for the region (50-60N, 10-20W) at 22 September 1982 (and therefore valid for 20 September). a) near 300hPa, b) near 850hPa.

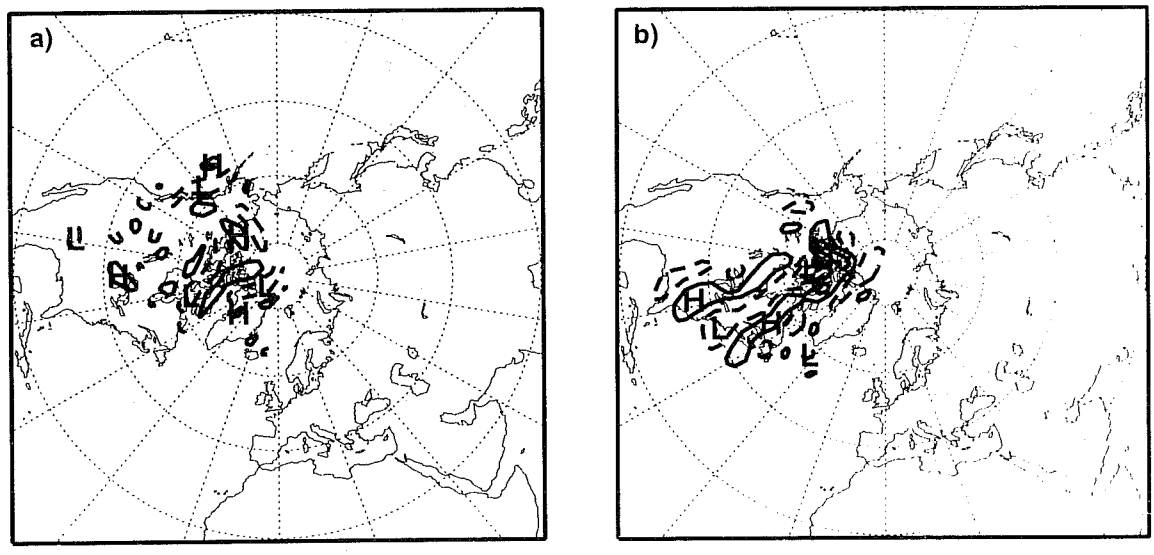

Fig. 14 Streamfunction for initial 96-hour singular vector optimised for the region (50-60N, 10-20W) at 24 September 1982 (and therefore valid for 20 September). a) near 300hPa, b) near 850hPa.

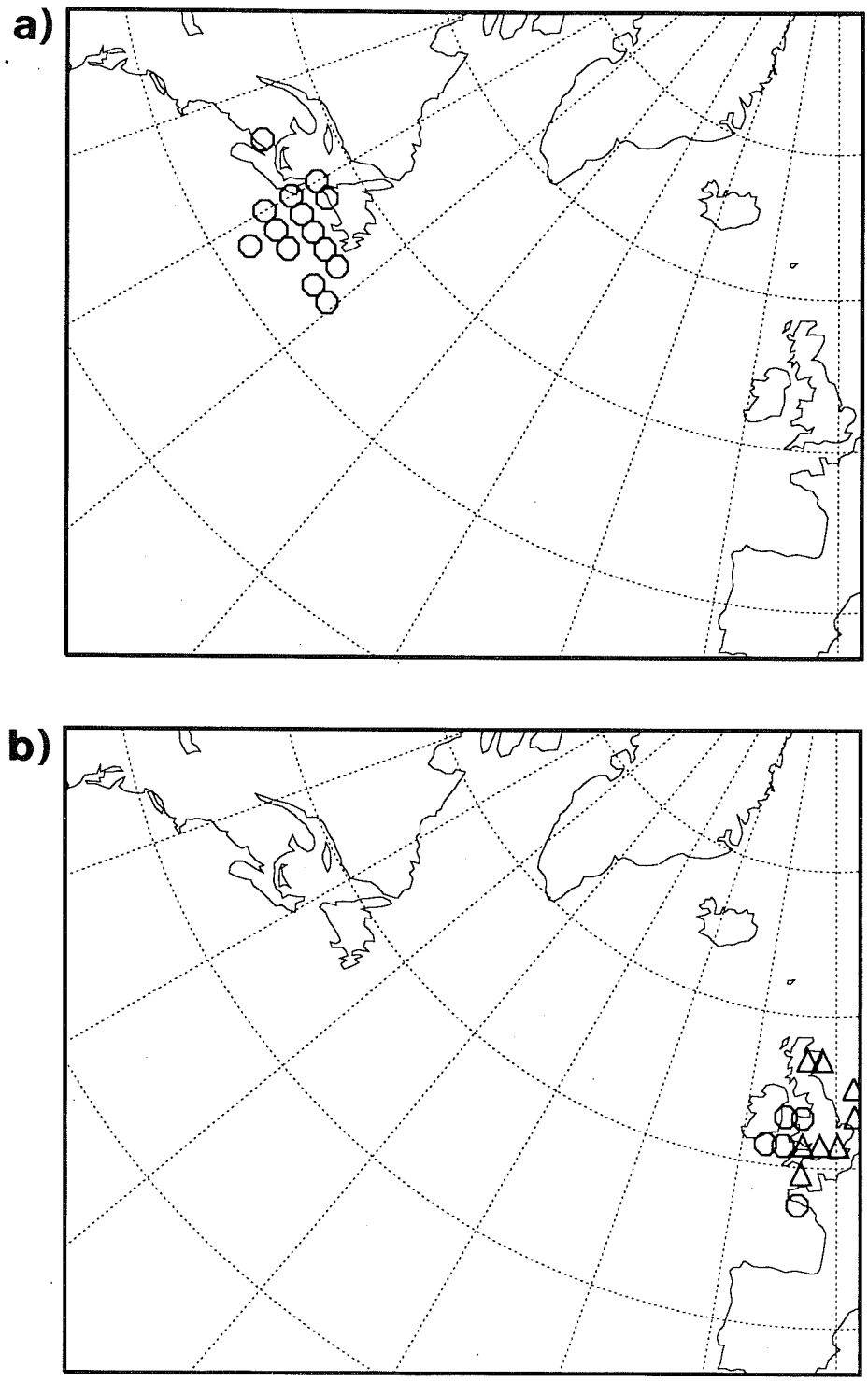

Fig. 15 Targets for adaptive observations based on 48-hour energy-metric singular vectors optimised for the FASTEX intensive observation area over the eastern Atlantic. The symbols show gridpoints where the vorticity of any of the first four singular vectors (weighted by the corresponding singular value) exceeds 0.7 times the maximum of the dominant singular vector. In a) (12z 23 December 1996), the target region is given only by the first singular vector (circles). In b) (12z 30 December 1996), the target region is defined from both the first (circles) and second (triangles) singular vectors. The difference in targeting regions between a) and b) reflects the changing large-scale atmospheric circulation between 23-30 December. *(Figure produced by A.Montani, Reading University, UK.)*